

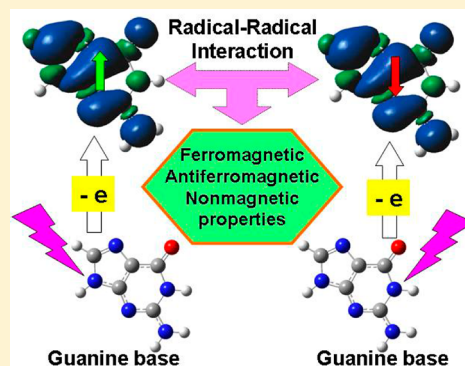
Radical–Radical Interactions among Oxidized Guanine Bases Including Guanine Radical Cation and Dehydrogenated Guanine Radicals

Jing Zhao, Mei Wang, Hongfang Yang, Meng Zhang, Ping Liu, and Yuxiang Bu*

School of Chemistry and Chemical Engineering, Shandong University, Jinan, 250100, People's Republic of China

S Supporting Information

ABSTRACT: We present here a theoretical investigation of the structural and electronic properties of di-ionized GG base pairs ($G^{\bullet+}G^{\bullet+}$, $G(-H1)^{\bullet}G^{\bullet+}$, and $G(-H1)^{\bullet}G(-H1)^{\bullet}$) consisting of the guanine cation radical ($G^{\bullet+}$) and/or dehydrogenated guanine radical ($G(-H1)^{\bullet}$) using density functional theory calculations. Different coupling modes (Watson–Crick/WC, Hoogsteen/Hoog, and minor groove/min hydrogen bonding, and π – π stacking modes) are considered. We infer that a series of $G^{\bullet+}G^{\bullet+}$ complexes can be formed by the high-energy radiation. On the basis of density functional theory and complete active space self-consistent (CASSCF) calculations, we reveal that in the H-bonded and N–N cross-linked modes, $(G^{\bullet+}G^{\bullet+})_{WC}$, $(G(-H1)^{\bullet}G(-H1)^{\bullet})_{WC}$, $(G(-H1)^{\bullet}G(-H1)^{\bullet})_{minI}$, and $(G(-H1)^{\bullet}G(-H1)^{\bullet})_{minIII}$ have the triplet ground states; $(G^{\bullet+}G^{\bullet+})_{HoogI}$, $(G(-H1)^{\bullet}G^{\bullet+})_{WC}$, $(G(-H1)^{\bullet}G^{\bullet+})_{HoogI}$, $(G(-H1)^{\bullet}G^{\bullet+})_{minI}$, $(G(-H1)^{\bullet}G^{\bullet+})_{minII}$, and $(G(-H1)^{\bullet}G(-H1)^{\bullet})_{minII}$ possess open-shell broken-symmetry diradical-characterized singlet ground states; and $(G^{\bullet+}G^{\bullet+})_{HoogII}$, $(G^{\bullet+}G^{\bullet+})_{minI}$, $(G^{\bullet+}G^{\bullet+})_{minII}$, $(G^{\bullet+}G^{\bullet+})_{minIII}$, $(G^{\bullet+}G^{\bullet+})_{HoHo}$, $(G(-H1)^{\bullet}G^{\bullet+})_{minIII}$, $(G(-H1)^{\bullet}G^{\bullet+})_{HoHo}$, and $(G(-H1)^{\bullet}G(-H1)^{\bullet})_{HoHo}$ are the closed-shell systems. For these H-bonded diradical complexes, the magnetic interactions are weak, especially in the diradical $G^{\bullet+}G^{\bullet+}$ series and $G(-H1)^{\bullet}G(-H1)^{\bullet}$ series. The magnetic coupling interactions of the diradical systems are controlled by intermolecular interactions (H-bond, electrostatic repulsion, and radical coupling). The radical–radical interaction in the π – π stacked di-ionized GG base pairs ($(G^{\bullet+}G^{\bullet+})_{\pi\pi}$, $(G(-H1)^{\bullet}G^{\bullet+})_{\pi\pi}$, and $(G(-H1)^{\bullet}G(-H1)^{\bullet})_{\pi\pi}$) are also considered, and the magnetic coupling interactions in these π – π stacked base pairs are large. This is the first theoretical prediction that some di-ionized GG base pairs possess diradical characters with variable degrees of ferromagnetic and antiferromagnetic characteristics, depending on the dehydrogenation characters of the bases and their interaction modes. Hopefully, this work provides some helpful information for the understanding of different structures and properties of the di-ionized GG base pairs.



1. INTRODUCTION

In the past decade, the issues of radiation damage to DNA, induced by ionizing radiation, chemical oxidation, photoionization, and photosensitization, have attracted considerable attention from the scientific community.^{1–4} Both theoretical and experimental explorations on this important subject have been directed an understanding of the underlying chemical mechanism during and after damage to DNA. It is known that exposure of DNA and related model compounds to high-energy radiation yields anion and cation radical species as the result of biphotonic excitation.^{5,6} The formation of these radicals among the DNA base pairs alter their structures and may lead to DNA damage or formation of lesions within DNA strands. The DNA damage could cause several life-degrading phenomena and diseases, such as cancer and aging.^{7,8}

Prior theoretical studies have been devoted to the energetics and structural features of both the closed shell,^{9,10} H-abstracted,¹¹ and deprotonated guanine–cytosine (G–C)¹² and adenine–uracil (A–U)¹³ base pairs, as well as the closed shell and H-abstracted^{14,15} individual DNA bases. Dulcic et al.^{16–18} found a strong radical pair EPR (electron paramagnetic

resonance) signal from the radical–radical interaction of two major radical species generated by losing or gaining the hydrogen atom in irradiated crystalline thymine at 77 K. Recently, Peoples et al.¹⁹ successfully investigated the diradical formation in calf thymus DNA films X-irradiated at 4 K using EPR. We note that in their study, the yield of trapped DNA radical pairs was found to be twice the number of radiation-induced double strand breaks (dsb's) measured in the same DNA sample by warming them at room temperature. Because the DNA films are amorphous, EPR spectrum of DNA showed no evidence of radical pairs, and they only set an upper limit to their formation. This difference between the fraction of trapped radical pairs and dsb's can be accounted for by invoking the double oxidation events, which are more probable in the high linear energy transfer (LET) radiation. The formation of radical pairs has been reported by experimental studies.^{20–22} The literature is rich with reports of trapped radicals in DNA

Received: April 29, 2013

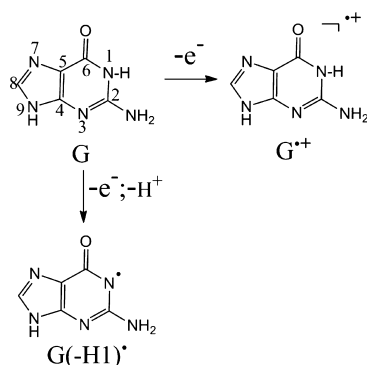
Revised: August 20, 2013

Published: August 21, 2013

irradiated by high LET radiation such as heavy-ions beams. Furthermore, the radiation-produced DNA base pair diradicals have also been reported.^{23,24} Pottiboyina and co-workers²³ investigated the theoretically possible formation of the hydrazine-like (N–N) cross-linked structures from the radical–radical reactions between DNA base pair diradicals that are likely to result from the interaction of high LET radiation. Their work provides thermodynamic and structural properties for the N–N cross-link radical–radical reactions. Seal et al.²⁴ studied the dehydrogenated guanine-cytosine diradical base pairs using the spin-flip broken symmetry method, and found antiferromagnetic (AFM) interactions in these G–C diradicals. They suggested that the H-bonds play a crucial role in determining the magnetic interactions in the G–C diradicals. To our knowledge, no theoretical study of the diradical character and magnetic property for the di-ionized GG base pairs has been reported so far.

We extend the research to explore the interactions of the di-ionized GG base pairs in this work. The di-ionized GG base pairs could be considered as the representative for studying radical–radical interaction of the oxidized mismatched base pairs. Herein, we intend to see when two radicals coexist at the same time in a system, whether these GG radical pairs have some interesting electronic properties. In general, the one-electron oxidation of guanine residues first produces the guanine radical cation ($G^{\bullet+}$), which is a harbinger of many pathological conditions in living cells as a result of its involvement in many diverse reactions.^{25–27} Additionally, it has been found that $G^{\bullet+}$ deprotonates quite rapidly in DNA at the N1–H site, leading to the formation of the guanine neutral radical ($G(-H)^{\bullet}$)^{28,29} with a rate constant of $1.8 \times 10^7 \text{ s}^{-1}$ at pH 7.0, which is another oxidized state in DNA damage. In fact, the prototropic equilibria of guanine cation radical have been characterized using electron spin resonance (ESR) spectroscopy and UV–vis spectra studies in DNA systems including monomers,²⁹ single-stranded DNA (ssDNA) oligomers,³⁰ and double-stranded DNA (dsDNA).^{31,32} Moreover, up to now, the UV–vis spectroscopy of the $G(-H)^{\bullet}$ in aqueous solution at ambient temperature has been extensively studied experimentally by Candeias and co-workers³³ in the monomer deoxyguanosine (dG), and Tagawa and co-workers^{28,34} in the dsDNA oligomer. Both experimental^{29,33} and theoretical^{35–37} studies have shown the primary deprotonation site to be the N1 position of guanine in an aqueous environment (Scheme 1).

Scheme 1. The Structures of Two Oxidized States of Guanine: Guanine Radical Cation ($G^{\bullet+}$) and N1-Dehydrogenated Guanine Radical ($G(-H)^{\bullet}$) and Atomic Numbering Schemes



Pulse radiolysis and laser photolysis experiments^{29,33} show that the $G^{\bullet+}$ form of dG has a pK_a of 3.9, and at pH = 7 the neutral oxidized radical ($G(-H)^{\bullet}$) is formed by rapid loss of the N1 proton. All in all, because of direct radiation damage and oxidation, hydrogen atoms in the base pair can be removed, which results in various neutral and cationic radicals.

The structures and properties of the $G^{\bullet+}$ – $G^{\bullet+}$, $G(-H)^{\bullet}$ – $G^{\bullet+}$, and $G(-H)^{\bullet}$ – $G(-H)^{\bullet}$ conformers (denoted by $G^{\bullet+}G^{\bullet+}$, $G(-H)^{\bullet}G^{\bullet+}$, and $G(-H)^{\bullet}G(-H)^{\bullet}$, respectively) have not been reported previously. Thus, in this work, we first investigate all possible structures of $G^{\bullet+}G^{\bullet+}$. Examination reveals that the first and second ionization potentials (IP_1 , IP_2) of various GG dimers are 6.55–7.54 eV (IP_1) and 10.06–11.25 eV (IP_2), respectively (Table 1). Clearly, these results imply the possibility of the formation of the two-electron-oxidized GG base pair and its deprotonated derivatives through high energy radiation or biphotonization. Over the past few years, the existence and stability of charged ion pairs in biological processes have gained increasing attention of researchers, primarily motivated by their important applications in biological processes. Recent experimental and theoretical studies^{38–42} have shown that the guanidinium cation can pair with each other in aqueous solution even though a strong repulsive electrostatic interaction is present between them, and the ion pair can be stabilized mainly by cavitation effects and quadrupole–quadrupole and dispersion interactions. In particular, Vazdar et al.³⁹ has proved that the existence of like-charge guanidinium–guanidinium contact ion pairs in water is established by ab initio molecular dynamics simulations. Moreover, Becker et al.^{43,44} claimed that for high-LET radiation such as α particles or heavier ion beams, a densely ionized track is formed where near neighbor molecules possess a much higher probability of ionization along with the formation of associated radicals. Further, the proximate radicals generated in these tracks may recombine to form new molecular species with unique structures with a high probability. Thus, it is conceivable that these $G^{\bullet+}G^{\bullet+}$ conformers could exist in an organism.

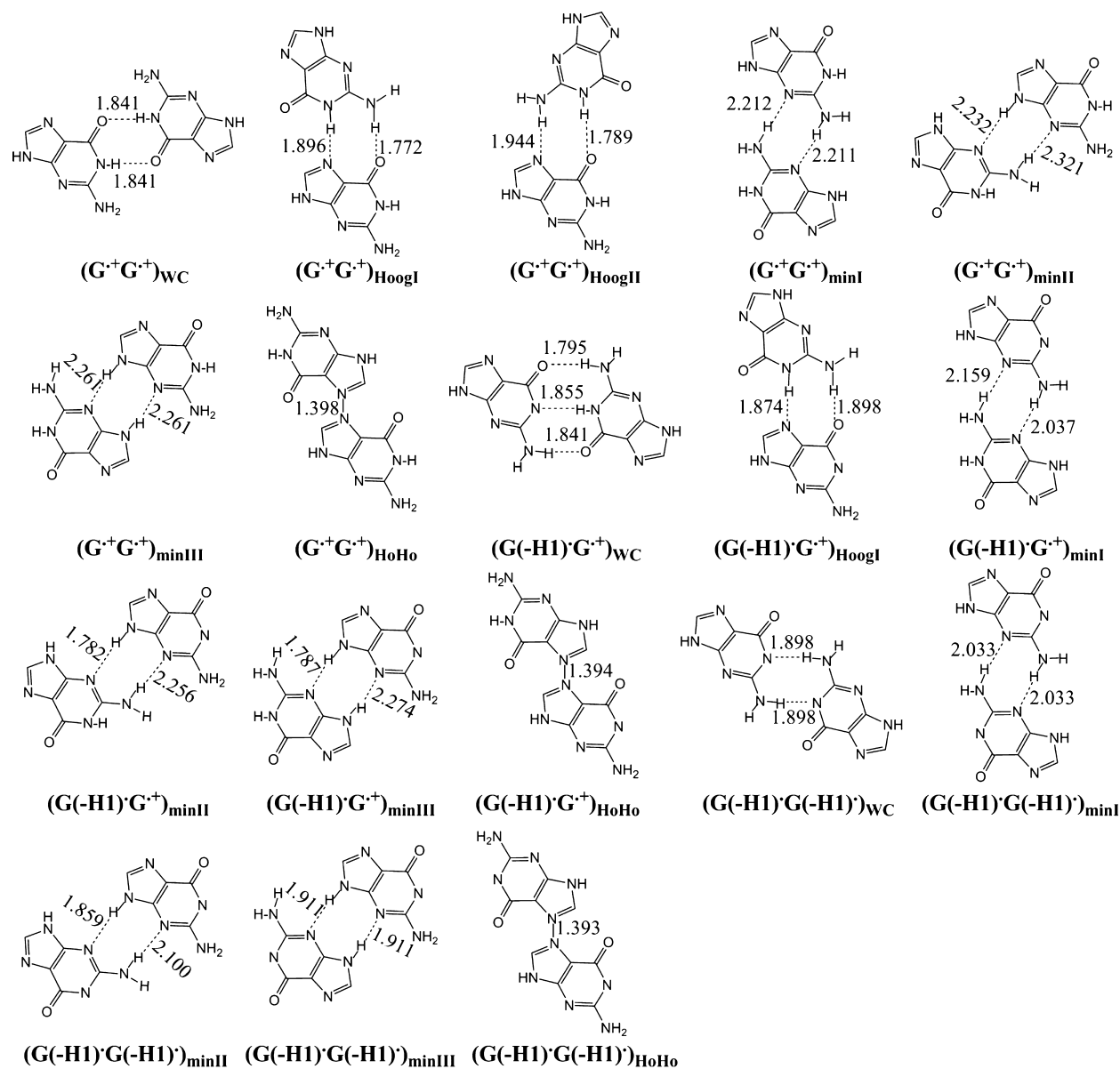
Until now, yet very little is reported for detecting the two-electron-oxidation induced DNA mismatched base pairs concerned over the diradical signals and magnetic properties. Examining radical interactions within DNA can promote the understanding of the structural and electronic properties of possible intermediates or products and even the two-electron oxidation mechanism of DNA at the atomistic and electronic levels.

2. COMPUTATIONAL METHODS

Geometry optimizations and property calculations of the hydrogen-bonded and N–N cross-linked two-electron oxidized GG base pairs were carried out using the unrestricted Becke's hybrid three-parameter UB3LYP⁴⁵ density functional approach with a 6-311+G* basis set. Vibrational frequency analyses were performed to confirm that all stationary points represent true minima on the potential energy surfaces. The binding energy of a di-ionized GG base pair is defined as $\Delta E = E_{\text{complex}} - E_{\text{base1}} - E_{\text{base2}}$, where E_{complex} , E_{base1} , and E_{base2} are the total energies of the base pair complex and two isolated $G^{\bullet+}$ and/or $G(-H)^{\bullet}$, respectively. The basis set superposition error (BSSE) corrections⁴⁶ were done using counterpoise method to obtain accurate binding energies. The relevant electronic properties including spin density distribution, highest occupied molecular orbital (HOMO), and lowest unoccupied molecular orbital (LUMO) were calculated. To examine the solvent effect, a

Table 1. The First Ionization Potentials (IP_1) and Second Ionization Potentials (IP_2) of $(GG)_{WC}$, $(GG)_{Hoogl}$, $(GG)_{HoogII}$, $(GG)_{minI}$, $(GG)_{minII}$, and $(GG)_{minIII}$ ^a

	$(GG)_{WC}$	$(GG)_{Hoogl}$	$(GG)_{HoogII}$	$(GG)_{minI}$	$(GG)_{minII}$	$(GG)_{minIII}$
IP_1	7.19	6.63	6.55	7.49	7.52	7.54
IP_2	10.06	10.48	10.96	11.17	11.21	11.25

^aAll energies are obtained at the B3LYP/6-311+G* level in eV.**Figure 1.** B3LYP/6-311+G*-optimized geometries for the hydrogen-bonded and N–N cross-linked $G^{\bullet+}G^{\bullet+}$ series, $G(-H1)^{\bullet}G^{\bullet+}$ series, and $G(-H1)^{\bullet}G(-H1)^{\bullet}$ series in the closed-shell singlet state. Distance in angstroms.

polarizable continuum model (PCM) with the dielectric constant of water ($\epsilon = 78.4$) was used. The single-point calculations at the B3LYP/6-311+G* level on the gas-phase optimized geometries were performed for these complexes. Because B3LYP does not account for dispersion interactions, the M06-2X method was used to study the π – π stacked structures, which was developed by Zhao and Truhlar and has also shown promise for noncovalent complexes.^{47,48}

Since these radically interacted systems exhibit noticeable radical characters, the magnetic coupling interactions are also explored. The magnetic coupling constant (J) between two spin

centers were calculated using a broken symmetry (BS) approach proposed by Noodleman^{49,50} within unrestricted density functional theory (DFT) framework. The positive and negative J values indicate the ferromagnetic (FM) and antiferromagnetic (AFM) properties between the two spin operators, respectively. The coupling constant formula proposed by Yamaguchi and co-workers^{51,52} is considered as the most appropriate formalism for estimating the magnetic exchange coupling constants of diradicals. The formula is written as

$$J = \frac{(E_{\text{BS}} - E_{\text{T}})}{\langle S^2 \rangle_{\text{T}} - \langle S^2 \rangle_{\text{BS}}}$$

where E_{BS} and E_{T} refer to the energies of the unrestricted BS singlet and triplet states, respectively. The $\langle S^2 \rangle_{\text{BS}}$ and $\langle S^2 \rangle_{\text{T}}$ denote the average spin square $\langle S^2 \rangle$ values for the BS and triplet states, respectively.

Considering that the unrestricted UB3LYP singlet calculation can only obtain the results similar to those at the restricted RB3LYP level for the singlet and does not really reflect the diradical character and the lowest state energies for the diradical molecules, the “guess=mix” keyword which can obtain an unrestricted broken spin-symmetry solution by mixing the near-energy low-lying triplet into the singlet state to yield the correct ground states is added in all optimizations.

The occupation number of the LUMO is a direct computational measure of the amount of diradical character. The perfect diradical characters are characterized by occupation numbers of 1.0 in HOMO and LUMO. The diradical character of these molecules was theoretically examined directly by the orbital occupation numbers from complete active space self-consistent field (CASSCF) method with 10 orbitals and 10 electrons in the active space by means of CASSCF(10,10).⁵³

All the calculations were carried out using the Gaussian 09 Program.⁵⁴

3. RESULTS AND DISCUSSION

3.1. Hydrogen-Bonded and N–N Cross-Linked $\text{G}^{+\bullet}\text{G}^{+\bullet}$, $\text{G}(-\text{H1})^+\text{G}^{+\bullet}$, and $\text{G}(-\text{H1})^+\text{G}(-\text{H1})^{\bullet}$ Complexes. Figure 1 provides the optimized geometries of the hydrogen-bonded and N–N cross-linked structures of the GG derivatives in the closed-shell singlet (CS) state. The corresponding open-shell BS singlet (BS) and triplet (T) states were also calculated. Their geometries were confirmed to be stable by optimizations and frequency calculations. According to the types of molecular monomer ($\text{G}^{+\bullet}$, and $\text{G}(-\text{H1})^{\bullet}$) and binding sites, these conformers are classified into three series: $\text{G}^{+\bullet}\text{G}^{+\bullet}$ series including $(\text{G}^{+\bullet}\text{G}^{+\bullet})_{\text{WC}/\text{Hoog}/\text{min}/\text{HoHo}}$, $\text{G}(-\text{H1})^+\text{G}^{+\bullet}$ series including $(\text{G}(-\text{H1})^+\text{G}^{+\bullet})_{\text{WC}/\text{Hoog}/\text{min}/\text{HoHo}}$, and $\text{G}(-\text{H1})^+\text{G}(-\text{H1})^{\bullet}$ series including $(\text{G}(-\text{H1})^+\text{G}(-\text{H1})^{\bullet})_{\text{WC}/\text{min}/\text{HoHo}}$. In these cases, the subscripts WC, Hoog, and min denote that the interactions occur in the Watson–Crick (WC), major and minor grooves of $\text{G}^{+\bullet}$ or $\text{G}(-\text{H1})^{\bullet}$, respectively, and the subscript HoHo represents the N7–N7 cross-linked species that is formed by the hydrazine-like covalent bond in the Hoogsteen (Ho) H-bond zones.

We also calculated the first and second ionization potentials for the hydrogen-bonded GG complexes $((\text{GG})_{\text{WC}}$, $(\text{GG})_{\text{HoogI}/\text{HoogII}}$, $(\text{GG})_{\text{minI}/\text{minII}/\text{minIII}}$), and the results reveal that the range of the first ionization potential is 6.55–7.54 eV, while that of the second ionization potential is 10.06–11.25 eV (Table 1). Clearly, these results imply that double ionization phenomena might occur in the GG base pairs along with the enhancement of radiation (such as α particles or heavier ion beams). The spin density surfaces of the one-electron oxidized $(\text{GG})_{\text{WC}}$, $(\text{GG})_{\text{HoogI}/\text{HoogII}}$ and $(\text{GG})_{\text{minI}/\text{minII}/\text{minIII}}$ base pairs are given in Figure 2. As expected, for one-electron oxidized $(\text{GG})_{\text{WC}}$, $(\text{GG})_{\text{minI}}$, $(\text{GG})_{\text{minII}}$ and $(\text{GG})_{\text{minIII}}$, spin densities distribute on the two G moieties equally. Consequently, we infer that for the second ionization, the hole still delocalizes on both G moieties equally. One interesting phenomenon occurs in one-electron oxidized $(\text{GG})_{\text{HoogI}}$ and $(\text{GG})_{\text{HoogII}}$ that is, the spin density localizes on one G piece. This means that when

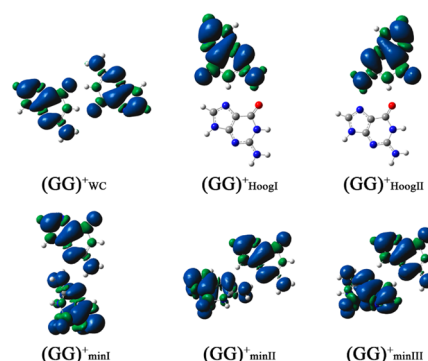


Figure 2. The spin density surfaces for the $(\text{GG})_{\text{WC}}^{+\bullet}$, $(\text{GG})_{\text{HoogI}}^{+\bullet}$, $(\text{GG})_{\text{HoogII}}^{+\bullet}$, $(\text{GG})_{\text{minI}}^{+\bullet}$, $(\text{GG})_{\text{minII}}^{+\bullet}$ and $(\text{GG})_{\text{minIII}}^{+\bullet}$.

$(\text{GG})_{\text{HoogI}}$ or $(\text{GG})_{\text{HoogII}}$ ionizes, the produced hole is merely trapped on one G. As is known, the second ionization potential of G is higher than the first ionization potential, and naturally, the second ionization in $(\text{GG})_{\text{HoogI}}$ or $(\text{GG})_{\text{HoogII}}$ will occur on the other G moiety. Additionally, we find that in the doubly ionized $(\text{GG})_{\text{WC}}$, $(\text{GG})_{\text{HoogI}/\text{HoogII}}$ and $(\text{GG})_{\text{minI}/\text{minII}/\text{minIII}}$ two positive charges distribute equally on both G moieties (1.0 for each), which further confirms the possibility of the formation of $\text{G}^{++}\text{G}^{++}$.

The binding energies of their ground states are shown in Figure 3, which ensure structural stabilities of these base pairs.

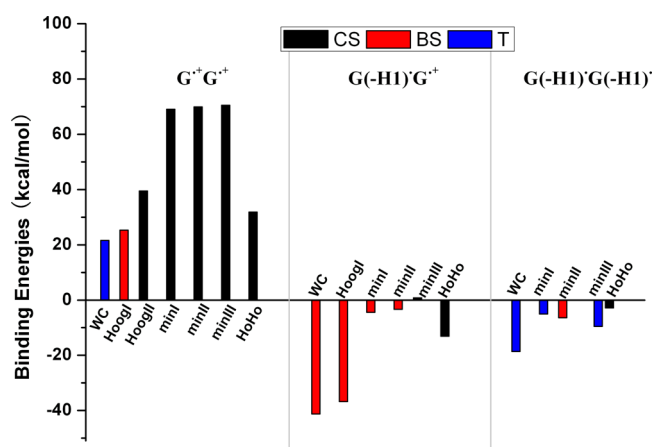


Figure 3. Binding energies of the $\text{G}^{+\bullet}\text{G}^{+\bullet}$ series, $\text{G}(-\text{H1})^+\text{G}^{+\bullet}$ series, and $\text{G}(-\text{H1})^+\text{G}(-\text{H1})^{\bullet}$ series in their corresponding ground states. The binding energies are obtained at the B3LYP/6-311+G* level of theory.

Our calculations indicate that the ground states of the $\text{G}(-\text{H1})^+\text{G}^{+\bullet}$ and $\text{G}(-\text{H1})^+\text{G}(-\text{H1})^{\bullet}$ complexes possess favorable binding energies. However, the binding energies of $\text{G}^{+\bullet}\text{G}^{+\bullet}$ are positive, suggesting that these $\text{G}^{+\bullet}\text{G}^{+\bullet}$ complexes are in high-energy metastable states. The vibrational frequencies show that these complexes are all minimum energy species on the potential energy surface, and considerable barriers can inhibit their dissociations. This indicates that these $\text{G}^{+\bullet}\text{G}^{+\bullet}$ are thermodynamically unstable, but they are kinetically favorable. In the following, we make a detailed analysis to obtain a basic understanding of the structural and electronic properties of these complexes.

A. $\text{G}^{+\bullet}\text{G}^{+\bullet}$ Series. These hydrogen-bonded and N–N cross-linked $\text{G}^{+\bullet}\text{G}^{+\bullet}$ complexes are displayed in Figure 1 and Figure S1–S10 (in the Supporting Information). From Figure 1, it is quite clear that a remarkable structural feature for

$(G^{\bullet+}G^{\bullet+})_{\text{HoHo}}$ is a short N–N contact between the two bases compared with the other base pairs. The cross-linked N–N distance is only 1.398 Å, a bond length of normal covalent bond, and it thus implies a covalent bonding interaction between the two bases through forming a N–N linkage. That is, the two radicals interact with each other, forming a covalent bond through linking two N7 of the two radical bases, as a result, leading to disappearance of the radical characters of the two bases. Clearly, this is distinctly different from all other binding modes, $(G^{\bullet+}G^{\bullet+})_{\text{WC/Hoogl/HooglII/minI/minII/minIII}}$, in which two bases are bound together through H-bonds and the formed base pairs exhibit variable radical characters. Undoubtedly, for the $(G^{\bullet+}G^{\bullet+})_{\text{WC/Hoogl/HooglII/minI/minII/minIII}}$ complexes, the intermolecular H-bonds play an important role in stabilizing conformers.

In the $(G^{\bullet+}G^{\bullet+})_{\text{WC}}$ case, the energy of the triplet state is lower than those of both the singlet states, implying that the system possesses a triplet as its ground state (Table 2). In

Table 2. Energies (kcal/mol) for the Single–Triplet Gaps ($\Delta E_{\text{(T-BS)}}$), Differences between the Open-Shell BS Singlet and Closed-Shell RB3LYP Solution ($\Delta E_{\text{(BS-CS)}}$), Spin Squared Values for the Open-Shell BS Singlet ($\langle S^2 \rangle$) of the $G^{\bullet+}G^{\bullet+}$, $G(-\text{H1})^{\bullet}G^{\bullet+}$, and $G(-\text{H1})^{\bullet}G(-\text{H1})^{\bullet}$ Series Calculated at the B3LYP/6-311+G* Level

$G^{\bullet+}G^{\bullet+}$	$\Delta E_{\text{(T-BS)}}$	$\Delta E_{\text{(BS-CS)}}$	$\langle S^2 \rangle$
$(G^{\bullet+}G^{\bullet+})_{\text{WC}}$	−0.001	−17.56	1.02
$(G^{\bullet+}G^{\bullet+})_{\text{Hoogl}}$	0.0006	−11.80	1.02
$(G^{\bullet+}G^{\bullet+})_{\text{HoHo}}$	53.42	0	0
$G(-\text{H1})^{\bullet}G^{\bullet+}$	$\Delta E_{\text{(T-BS)}}$	$\Delta E_{\text{(BS-CS)}}$	$\langle S^2 \rangle$
$(G(-\text{H1})^{\bullet}G^{\bullet+})_{\text{WC}}$	0.063	−13.94	1.02
$(G(-\text{H1})^{\bullet}G^{\bullet+})_{\text{Hoogl}}$	0.0006	−17.30	1.03
$(G(-\text{H1})^{\bullet}G^{\bullet+})_{\text{minI}}$	0.434	−7.17	0.88
$(G(-\text{H1})^{\bullet}G^{\bullet+})_{\text{HoHo}}$	45.85	0	0
$G(-\text{H1})^{\bullet}G(-\text{H1})^{\bullet}$	$\Delta E_{\text{(T-BS)}}$	$\Delta E_{\text{(BS-CS)}}$	$\langle S^2 \rangle$
$(G(-\text{H1})^{\bullet}G(-\text{H1})^{\bullet})_{\text{WC}}$	−0.003	−19.65	1.03
$(G(-\text{H1})^{\bullet}G(-\text{H1})^{\bullet})_{\text{minII}}$	0.003	−17.74	1.03
$(G(-\text{H1})^{\bullet}G(-\text{H1})^{\bullet})_{\text{HoHo}}$	56.60	0	0

detail, at the B3LYP level of theory, the energy of the triplet state is considerably lower than the closed-shell singlet state by 17.56 kcal/mol. Although the open-shell BS singlet state yielded by mixing the triplet into the singlet state is also considerably lower than the closed-shell singlet state, it is still slightly higher than and very close to the triplet (by only about 0.001 kcal/mol). This quite small energy gap (~ 0.001 kcal/mol) implies that the two spin electrons almost have no effect on each other, being in an unpaired state. In a word, according to the energy order of various spin states ($E_{\text{T}} < E_{\text{BS}} < E_{\text{CS}}$), the $(G^{\bullet+}G^{\bullet+})_{\text{WC}}$ has a triplet ground state, which has two unpaired electrons located on two separate sites but with the parallel spins. It is worthy to note that, for $(G^{\bullet+}G^{\bullet+})_{\text{WC}}$, the triplet ground state is energetically more favorable than the corresponding closed-shell singlet, which means that a full mixing by the triplet into the singlet can stabilize the singlet state to some extent. This observation can be also proved by the lower gap between the BS singlet and triplet states.

Although $(G^{\bullet+}G^{\bullet+})_{\text{WC}}$ possesses a triplet ground state, it is quite important to explore its other possible lower-lying states, especially the diradical character in the open-shell BS state. Given the fact that the open-shell BS state is a novel and interesting electronic state, its structural and electronic

properties for $(G^{\bullet+}G^{\bullet+})_{\text{WC}}$ need to be investigated. As can be seen in Table 2, the spin contamination for its singlet state is 1.02. As is known, the $\langle S^2 \rangle$ value of the standard BS singlet state for a diradical molecule is usually close to 1.0. Therefore, the value of $(G^{\bullet+}G^{\bullet+})_{\text{WC}}$ ($\langle S^2 \rangle = 1.02$) obviously means that the BS singlet state is the mixture of pure singlet ($\langle S^2 \rangle = 0.0$) and pure triplet state ($\langle S^2 \rangle = 2.0$). In short, our DFT calculations reveal that $(G^{\bullet+}G^{\bullet+})_{\text{WC}}$ possesses a significant diradical character when it is in the open-shell BS singlet state. Quantitatively, we could see from Table S4 that the LUMO occupation number of $(G^{\bullet+}G^{\bullet+})_{\text{WC}}$ is 1.00 at the CASSCF level, indicating that the percentage of the diradical character is estimated to be about 100%.^{55–57} This high agreement between the CASSCF and DFT results further confirm a significant diradical character for $(G^{\bullet+}G^{\bullet+})_{\text{WC}}$.

For $(G^{\bullet+}G^{\bullet+})_{\text{Hoogl}}$, our unrestricted DFT calculations lead to an open-shell BS singlet diradical ground state with the significantly large amount of diradical character, which implies that its open-shell BS singlet ground state is energetically favorable than the corresponding closed-shell singlet and triplet state. In Table 2, we note that $(G^{\bullet+}G^{\bullet+})_{\text{Hoogl}}$ has obvious diradical character (spin contamination, $\langle S^2 \rangle = 1.02$). Here, its LUMO occupation number is calculated to be 0.995 and consequently, the amount of the diradical character is 99.5% (Table S4). The CASSCF-calculated results (0.995, the LUMO occupation number) is in perfect accord with the unrestricted DFT calculations (1.02 as the spin contamination), and both reveal the perfect diradical character. In short, the results indicate that the $(G^{\bullet+}G^{\bullet+})_{\text{Hoogl}}$ structure considered here possesses a well-defined open-shell BS singlet ground state with diradical character.

In addition, the $(G^{\bullet+}G^{\bullet+})_{\text{HoHo}}$ structure is also calculated with the “guess=mix” keyword, but we observe that the spin contamination for the obtained conformer is zero ($\langle S^2 \rangle = 0$) and the energy of the alpha singly occupied molecular orbital (SOMO(α)) is equal to that of SOMO(β), which shows that the BS state is a pure closed-shell singlet state (Table 2). Therefore, for $(G^{\bullet+}G^{\bullet+})_{\text{HoHo}}$, there is only closed-shell singlet and triplet states. In this case, the closed-shell singlet state is 53.42 kcal/mol lower in energy than the corresponding triplet state, and it confirms that $(G^{\bullet+}G^{\bullet+})_{\text{HoHo}}$ favors the closed-shell singlet ground state. Similar phenomena occur in $(G^{\bullet+}G^{\bullet+})_{\text{HooglII}}$, $(G^{\bullet+}G^{\bullet+})_{\text{minIV}}$, $(G^{\bullet+}G^{\bullet+})_{\text{minII}}$, and $(G^{\bullet+}G^{\bullet+})_{\text{minIII}}$, which possess the CS states as their ground states, too. As shown in Figure 1, the bond lengths of N...H–N and N–H...N in the $(G^{\bullet+}G^{\bullet+})_{\text{minI}}$ are 2.212 and 2.211 Å, respectively, and both of them are longer than the H-bonds in the $(G^{\bullet+}G^{\bullet+})_{\text{WC}}$ ($R_{\text{O...H-N}} = 1.841$ Å). Similar situations occur in $(G^{\bullet+}G^{\bullet+})_{\text{minII}}$ and $(G^{\bullet+}G^{\bullet+})_{\text{minIII}}$ (2.232, 2.321 Å for $(G^{\bullet+}G^{\bullet+})_{\text{minII}}$ and 2.261, 2.261 Å for $(G^{\bullet+}G^{\bullet+})_{\text{minIII}}$). For $(G^{\bullet+}G^{\bullet+})_{\text{HooglII}}$, there is repulsion interaction between the two carboxyl oxygen atoms. Additionally, for those complexes above, we also take their stabilities into account. From Figure 3, we can find that, among these different optimized $G^{\bullet+}G^{\bullet+}$ complexes considered here, the stabilities of them follow the order $(G^{\bullet+}G^{\bullet+})_{\text{WC}}^{\text{T}} > (G^{\bullet+}G^{\bullet+})_{\text{Hoogl}}^{\text{BS}} > (G^{\bullet+}G^{\bullet+})_{\text{HoHo}}^{\text{CS}} > (G^{\bullet+}G^{\bullet+})_{\text{HooglII}}^{\text{CS}} > (G^{\bullet+}G^{\bullet+})_{\text{minI}}^{\text{CS}} > (G^{\bullet+}G^{\bullet+})_{\text{minII}}^{\text{CS}} > (G^{\bullet+}G^{\bullet+})_{\text{minIII}}^{\text{CS}}$. Clearly, for the $G^{\bullet+}G^{\bullet+}$ series, the $(G^{\bullet+}G^{\bullet+})_{\text{WC}}^{\text{T}}$ is found to be the most stable. In addition, it should be noted that when these species are in their closed-shell singlet states, the binding strengths for $(G^{\bullet+}G^{\bullet+})_{\text{minIV}}^{\text{CS}}$, $(G^{\bullet+}G^{\bullet+})_{\text{minII}}^{\text{CS}}$, and $(G^{\bullet+}G^{\bullet+})_{\text{minIII}}^{\text{CS}}$ (69.10, 69.94, and 70.50 kcal/mol) are relatively weaker than those of $(G^{\bullet+}G^{\bullet+})_{\text{WC}}^{\text{CS}}$ and $(G^{\bullet+}G^{\bullet+})_{\text{Hoogl}}^{\text{CS}}$ (39.16 and 37.49 kcal/

mol). The H-bonding attraction, electrostatic repulsion, and radical coupling interaction play important roles in stabilizing $(G^{\bullet+}G^{\bullet+})_{\text{Hoogl}}$, $(G^{\bullet+}G^{\bullet+})_{\text{minI}}$, $(G^{\bullet+}G^{\bullet+})_{\text{minII}}$, and $(G^{\bullet+}G^{\bullet+})_{\text{minIII}}$. In these four complexes, due to the mutual balance of these three interactions and the weak binding strength, their corresponding structures of the triplet state convert into the other conformers.

To visualize their interesting diradical character, and to give more insight into the nature of the open-shell BS singlet state, the frontier molecular orbitals and spin density distributions were determined. These orbitals further confirm the diradical character. The SOMOs and spin density distributions of this $G^{\bullet+}G^{\bullet+}$ series were calculated (as shown in the Supporting Information) and only those of $(G^{\bullet+}G^{\bullet+})_{\text{WC}}$ are shown for an illustration in Figures 4 and 5. It is evident that the unpaired

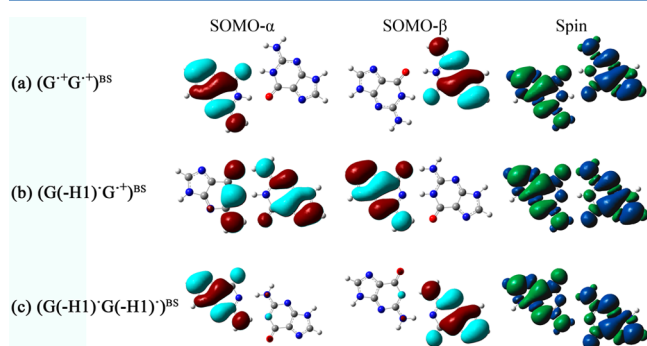


Figure 4. The SOMOs and spin density maps of open-shell BS singlet (a) $(G^{\bullet+}G^{\bullet+})_{\text{WC}}$, (b) $(G(-H1)G^{\bullet+})_{\text{WC}}$, and (c) $(G(-H1)G(-H1))_{\text{WC}}$. Blue and green surfaces of the spin density maps denote α and β spin density, respectively.

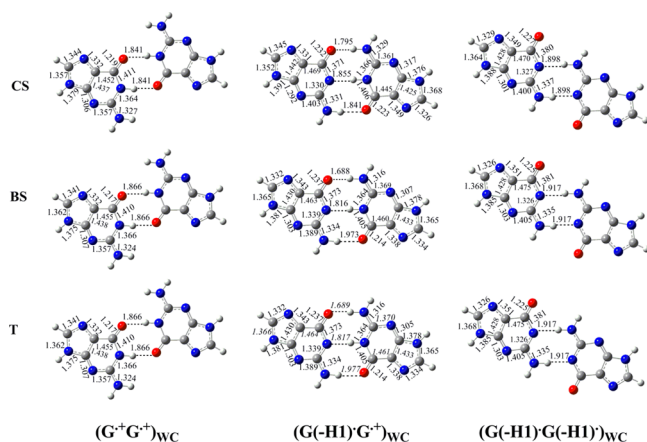


Figure 5. Optimized geometries with the corresponding bond lengths (Å) for $(G^{\bullet+}G^{\bullet+})_{\text{WC}}$, $(G(-H1)G^{\bullet+})_{\text{WC}}$, and $(G(-H1)G(-H1))_{\text{WC}}$.

electrons are basically located on the two radical rings. The spin density localizes on the whole fragments of the diradical base pairs but being spin-up and spin-down distinguishable. They are strong evidence of the diradical character of the open-shell singlet state.

We also calculated the magnetic coupling constants J . As shown in Table 3, the J values of the $(G^{\bullet+}G^{\bullet+})_{\text{WC}}$ and $(G^{\bullet+}G^{\bullet+})_{\text{Hoogl}}$ are 0.31 and -0.22 cm^{-1} , respectively, suggesting that they exhibit slight FM and AFM characters. This is consistent with the quite small energy gaps between the singlet and triplet (0.001 kcal/mol for $(G^{\bullet+}G^{\bullet+})_{\text{WC}}$ and -0.0006 kcal/

mol for $(G^{\bullet+}G^{\bullet+})_{\text{Hoogl}}$), indicating that the interaction between the two $G^{\bullet+}$ radicals is very weak. However, for $(G^{\bullet+}G^{\bullet+})_{\text{Hoogl}}$, $(G^{\bullet+}G^{\bullet+})_{\text{minI}}$, $(G^{\bullet+}G^{\bullet+})_{\text{minII}}$, $(G^{\bullet+}G^{\bullet+})_{\text{minIII}}$, and $(G^{\bullet+}G^{\bullet+})_{\text{HoHo}}$, there exists no magnetic property in them. In a word, the radical pairs of $G^{\bullet+}G^{\bullet+}$ with different binding modes only show slightly magnetic character (FM or AFM).

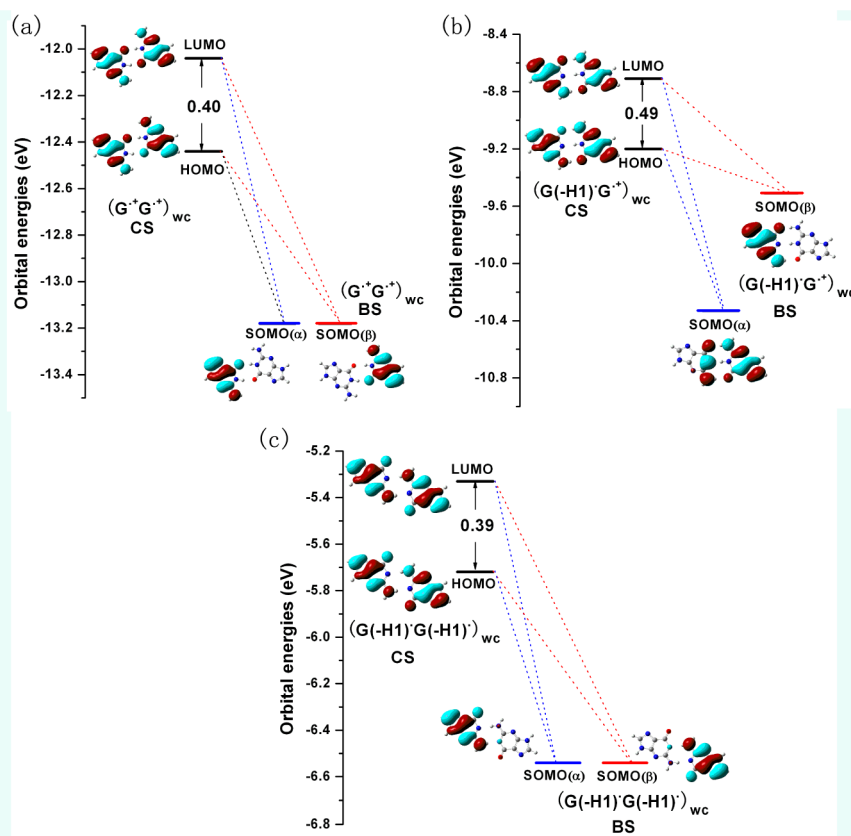
B. $G(-H1)G^{\bullet+}$ Series. For $(G(-H1)G^{\bullet+})_{\text{WC}}$, $(G(-H1)G^{\bullet+})_{\text{Hoogl}}$ and $(G(-H1)G^{\bullet+})_{\text{minI}}$, it turns out that the open-shell BS singlet states are lower by 0.063, 0.0006, and 0.434 kcal/mol than the corresponding triplet states (Table 2). These values imply that the $(G(-H1)G^{\bullet+})_{\text{minI}}$ has the largest coupling, followed by $(G(-H1)G^{\bullet+})_{\text{WC}}$ and $(G(-H1)G^{\bullet+})_{\text{Hoogl}}$. The open-shell BS singlet states are 13.94, 17.30, and 7.17 kcal/mol lower in energies than the closed-shell singlet states for $(G(-H1)G^{\bullet+})_{\text{WC}}$, $(G(-H1)G^{\bullet+})_{\text{Hoogl}}$ and $(G(-H1)G^{\bullet+})_{\text{minI}}$, respectively. Correspondingly, the spin contaminations $\langle S^2 \rangle$ of their open-shell BS states are 1.02, 1.03 and 0.88, respectively, implying that the BS singlet states are a mixture of pure singlet and pure triplet states (see Table 2). Quantitatively, the LUMO occupation numbers (0.984, 0.999, and 0.985) and the percentages of the diradical characters (98.4%, 99.9% and 98.5%) confirm the open-shell BS singlet diradical nature for $(G(-H1)G^{\bullet+})_{\text{WC}}$, $(G(-H1)G^{\bullet+})_{\text{Hoogl}}$ and $(G(-H1)G^{\bullet+})_{\text{minI}}$ (shown in Table S4). The SOMOs and spin density distributions of these three structures further reveal that they possess diradical character when they are in the open-shell singlet state (only those of $(G(-H1)G^{\bullet+})_{\text{WC}}$ are shown in Figure 4 and the others are given in the Supporting Information). Similar analyses reveal that $(G(-H1)G^{\bullet+})_{\text{minII}}$, $(G(-H1)G^{\bullet+})_{\text{minIII}}$, and $(G(-H1)G^{\bullet+})_{\text{HoHo}}$ possess the open-shell BS singlet, closed-shell singlet and closed-shell singlet as their ground states, respectively. The energy calculations reveal that the order of stabilities for these $G(-H1)G^{\bullet+}$ complexes is $(G(-H1)G^{\bullet+})_{\text{WC}}^{\text{BS}} > (G(-H1)G^{\bullet+})_{\text{Hoogl}}^{\text{BS}} > (G(-H1)G^{\bullet+})_{\text{minI}}^{\text{CS}} > (G(-H1)G^{\bullet+})_{\text{minII}}^{\text{BS}} > (G(-H1)G^{\bullet+})_{\text{minIII}}^{\text{CS}} > (G(-H1)G^{\bullet+})_{\text{HoHo}}^{\text{BS}}$.

As shown in Table 3, the magnetic exchange coupling constant J of $(G(-H1)G^{\bullet+})_{\text{WC}}$, $(G(-H1)G^{\bullet+})_{\text{Hoogl}}$ and $(G(-H1)G^{\bullet+})_{\text{minI}}$ are -22.02 , -0.81 , and -132.64 cm^{-1} , respectively, which indicate their AFM character and confirm their open-shell BS singlet diradical ground states. According to the calculated J values, we could see that the $G(-H1)G^{\bullet+}$ complexes exhibit different degrees of magnetic characters. In detail, the $(G(-H1)G^{\bullet+})_{\text{minI}}$ shows obvious AFM character with the largest J value, and the J values of $(G(-H1)G^{\bullet+})_{\text{WC}}$, $(G(-H1)G^{\bullet+})_{\text{Hoogl}}$ and $(G(-H1)G^{\bullet+})_{\text{minII}}$ exhibit AFM character. For $(G(-H1)G^{\bullet+})_{\text{minIII}}$ and $(G(-H1)G^{\bullet+})_{\text{HoHo}}$, they do not possess magnetic property.

C. $G(-H1)G(-H1)$ Series. For $(G(-H1)G(-H1))_{\text{WC}}$, the values of $\Delta E_{(\text{T-BS})}$ and $\Delta E_{(\text{BS-CS})}$ are -0.003 kcal/mol and -19.65 kcal/mol , respectively, which indicates that the $(G(-H1)G(-H1))_{\text{WC}}$ possesses a triplet ground state. Clearly, the triplet state is a bit lower than the open-shell BS singlet state, and thus the electronic character of the open-shell BS singlet state for the $(G(-H1)G(-H1))_{\text{WC}}$ is also investigated. For $(G(-H1)G(-H1))_{\text{minII}}$, its singlet–triplet gap is 0.003 kcal/mol (triplet over singlet), while its closed-shell RB3LYP solution is 17.74 kcal/mol above the corresponding open-shell BS singlet state, clearly implying that it has an open-shell BS singlet ground state. In both $(G(-H1)G(-H1))_{\text{WC}}$ and $(G(-H1)G(-H1))_{\text{minII}}$, the spin contaminations of their singlet state are very close to the perfect 1.0 ($\langle S^2 \rangle = 1.03, 1.03$), which clearly confirm their open-shell BS singlet diradical character. In

Table 3. Calculated Energies (a.u.), the Spin Contamination $\langle S^2 \rangle$ Values, and Intermolecular Magnetic Exchange Coupling Constants J of the $G^{\bullet+}G^{\bullet+}$, $G(-H1)^{\bullet}G^{\bullet+}$, and $G(-H1)^{\bullet}G(-H1)^{\bullet}$ Series Calculated at the B3LYP/6-311+G* Level

$G^{\bullet+}G^{\bullet+}$	$E_T (\langle S^2 \rangle)$	$E_{BS} (\langle S^2 \rangle)$	$J (\text{cm}^{-1})$
$(G^{\bullet+}G^{\bullet+})_{WC}$	−1084.802081 (2.02)	−1084.802079 (1.02)	0.31
$(G^{\bullet+}G^{\bullet+})_{Hoogl}$	−1084.796108 (2.02)	−1084.796109 (1.02)	−0.22
$(G^{\bullet+}G^{\bullet+})_{HoHo}$	−1084.703201 (2.02)	−1084.788334 (0)	0
$G(-H1)^{\bullet}G^{\bullet+}$	$E_T (\langle S^2 \rangle)$	$E_{BS} (\langle S^2 \rangle)$	$J (\text{cm}^{-1})$
$(G(-H1)^{\bullet}G^{\bullet+})_{WC}$	−1084.527152 (2.02)	−1084.527253 (1.02)	−22.02
$(G(-H1)^{\bullet}G^{\bullet+})_{Hoogl}$	−1084.519758 (2.03)	−1084.519759 (1.03)	−0.18
$(G(-H1)^{\bullet}G^{\bullet+})_{minI}$	−1084.467357 (2.03)	−1084.468049 (0.88)	−132.64
$(G(-H1)^{\bullet}G^{\bullet+})_{HoHo}$	−1084.411303 (2.00)	−1084.484378 (0)	0
$G(-H1)^{\bullet}G(-H1)^{\bullet}$	$E_T (\langle S^2 \rangle)$	$E_{BS} (\langle S^2 \rangle)$	$J (\text{cm}^{-1})$
$(G(-H1)^{\bullet}G(-H1)^{\bullet})_{WC}$	−1084.115219 (2.03)	−1084.115215 (1.03)	0.81
$(G(-H1)^{\bullet}G(-H1)^{\bullet})_{minII}$	−1084.095527 (2.03)	−1084.095531 (1.03)	−0.90
$(G(-H1)^{\bullet}G(-H1)^{\bullet})_{HoHo}$	−1084.092299 (2.02)	−1084.002094 (0)	0

**Figure 6.** Molecular orbital energy levels of the open-shell BS singlet states of (a) $(G^{\bullet+}G^{\bullet+})_{WC}$, (b) $(G(-H1)^{\bullet}G^{\bullet+})_{WC}$, and (c) $(G(-H1)^{\bullet}G(-H1)^{\bullet})_{WC}$ base pairs. The HOMO–LUMO gaps of the closed-shell diradicals are labeled, and the frontier orbitals are also represented here.

addition, the CASSCF calculations indicate that their LUMO occupation numbers are 1.00 and 0.993 with the amount of the diradical characters of 100% and 99.3% (Table S4). The SOMOs and spin density distributions of $(G(-H1)^{\bullet}G(-H1)^{\bullet})_{WC}$ and $(G(-H1)^{\bullet}G(-H1)^{\bullet})_{minII}$ have represented their open-shell BS singlet diradical nature visually and intuitively (as shown in Figure 4 and in the Supporting Information). From Table 3, it should be noted that the J values of $(G(-H1)^{\bullet}G(-H1)^{\bullet})_{WC}$ and $(G(-H1)^{\bullet}G(-H1)^{\bullet})_{minII}$ are 0.81 and -0.90 cm^{-1} , respectively, indicating slight FM and AFM character.

As for $(G(-H1)^{\bullet}G(-H1)^{\bullet})_{minIII}$, there are only the closed-shell singlet and triplet state conformers. Meanwhile, in this case, the triplet state is lower than the closed-shell singlet state by 17.71 kcal/mol, implying that the lowest-energy spin state is

a triplet state. For $(G(-H1)^{\bullet}G(-H1)^{\bullet})_{HoHo}$, the $\Delta E_{(T-CS)}$ (56.60 kcal/mol, triplet over CS singlet) combined with the spin contamination ($\langle S^2 \rangle \geq 0$) means that the closed-shell singlet state is the stable ground state. For $(G(-H1)^{\bullet}G(-H1)^{\bullet})_{minI}$, it possesses the triplet ground state.

In a word, we can see that $G(-H1)^{\bullet}G(-H1)^{\bullet}$ in different binding modes possess different spin states in their ground states. $(G(-H1)^{\bullet}G(-H1)^{\bullet})_{WC}$, $(G(-H1)^{\bullet}G(-H1)^{\bullet})_{minI}$, $(G(-H1)^{\bullet}G(-H1)^{\bullet})_{minII}$, and $(G(-H1)^{\bullet}G(-H1)^{\bullet})_{minIII}$ show different magnetic nature (FM, AFM, respectively). Finally, the DFT calculations show that the binding strength follows the sequence $(G(-H1)^{\bullet}G(-H1)^{\bullet})_{WC}^T > (G(-H1)^{\bullet}G(-H1)^{\bullet})_{minIII}^T > (G(-H1)^{\bullet}G(-H1)^{\bullet})_{minII}^{BS} > (G(-H1)^{\bullet}G(-H1)^{\bullet})_{minI}^T > (G(-$

$\text{H1})\cdot\text{G}(\text{-H1})\cdot^{\text{CS}}_{\text{HoHo}}$. Similar to $\text{G}^{\bullet+}\text{G}^{\bullet+}$, the strongest binding is the triplet state of $(\text{G}(\text{-H1})\cdot\text{G}(\text{-H1})\cdot)_{\text{WC}}$.

On the whole, the magnetic interactions of these hydrogen-bonded $\text{G}^{\bullet+}\text{G}^{\bullet+}$, $\text{G}(\text{-H1})\cdot\text{G}^{\bullet+}$, and $\text{G}(\text{-H1})\cdot\text{G}(\text{-H1})\cdot$ are weak. Thus, we observe their structure changes of the closed-shell singlet, open-shell BS singlet, and triplet states. Figure 5 provides the optimized geometries of $(\text{G}^{\bullet+}\text{G}^{\bullet+})_{\text{WC}}$, $(\text{G}(\text{-H1})\cdot\text{G}^{\bullet+})_{\text{WC}}$, and $(\text{G}(\text{-H1})\cdot\text{G}(\text{-H1})\cdot)_{\text{WC}}$ (see the Supporting Information for others). It can be seen that the bond length differences between the closed-shell singlet and open-shell states are no more than 0.1 Å. In addition, for $(\text{G}^{\bullet+}\text{G}^{\bullet+})_{\text{WC}}$ and $(\text{G}(\text{-H1})\cdot\text{G}(\text{-H1})\cdot)_{\text{WC}}$, it can be found that the structure of the open-shell BS singlet is same as that of the corresponding triplet. In the $(\text{G}(\text{-H1})\cdot\text{G}^{\bullet+})_{\text{WC}}$ case, the open-shell BS singlet and triplet states have very similar geometries with a maximal bond length difference of 0.004 Å. In other words, the geometries of these two open-shell spin states are of little difference, which indicate that these two spin electrons basically have no effect on each other.

We still select the $(\text{G}^{\bullet+}\text{G}^{\bullet+})_{\text{WC}}$, $(\text{G}(\text{-H1})\cdot\text{G}^{\bullet+})_{\text{WC}}$, and $(\text{G}(\text{-H1})\cdot\text{G}(\text{-H1})\cdot)_{\text{WC}}$ as the target models for further analyses. Additionally, the HOMO–LUMO gaps of the $(\text{G}^{\bullet+}\text{G}^{\bullet+})_{\text{WC}}$, $(\text{G}(\text{-H1})\cdot\text{G}^{\bullet+})_{\text{WC}}$, and $(\text{G}(\text{-H1})\cdot\text{G}(\text{-H1})\cdot)_{\text{WC}}$ base pairs are analyzed to explain why the open-shell states are more favorable than the closed-shell singlet states. As shown in Figure 6, the calculated HOMO–LUMO gaps of the $(\text{G}^{\bullet+}\text{G}^{\bullet+})_{\text{WC}}$, $(\text{G}(\text{-H1})\cdot\text{G}^{\bullet+})_{\text{WC}}$, and $(\text{G}(\text{-H1})\cdot\text{G}(\text{-H1})\cdot)_{\text{WC}}$ in their closed-shell singlet states are only 0.40, 0.49, and 0.39 eV, respectively. It can be seen that the gaps are so low that an electron is prone to promotion from HOMO to LUMO.⁴⁶ The HOMO and LUMO of the closed-shell singlet states and SOMOs of the open-shell BS singlet states for the three representative conformers are also displayed in Figure 6. It can be observed that the SOMOs are formed by a combination of the HOMO and LUMO, and the energies decrease, stabilizing the system. The results reveal the essence of the fact that the open-shell states are far more stable than the closed-shell states. This explains why diradical character easy to occur.

In order to further explain the magnetic coupling interaction, we have made the molecular orbital analysis and spin density distribution analysis of the triplet states for $(\text{G}^{\bullet+}\text{G}^{\bullet+})_{\text{WC}}$, $(\text{G}(\text{-H1})\cdot\text{G}^{\bullet+})_{\text{WC}}$, and $(\text{G}(\text{-H1})\cdot\text{G}(\text{-H1})\cdot)_{\text{WC}}$. According to Hoffmann's approach, the two singly occupied orbitals of the radical centers can form a symmetric magnetic orbital (ϕ_s) and an antisymmetric magnetic orbital (ϕ_a). The ϕ_s and ϕ_a are expressed by the following equation:

$$\phi_s = \varphi(1) + \varphi(2) \quad \phi_a = \varphi(1) - \varphi(2)$$

Moreover, on the basis of Hoffmann's theory, the magnetic interaction is defined as

$$J = k_{ab} - \frac{|\varepsilon_a - \varepsilon_s|^2}{J_{aa} - J_{ab}}$$

where k_{ab} , J_{aa} , J_{ab} are the two-electron integrals of the orbital localization, and ε_a , ε_s denote the energies of two singly occupied molecular orbitals, respectively. These indicate that the energy gap $\Delta = |\varepsilon_a - \varepsilon_s|$ is the main factor in magnetic interaction. When the configuration parameter changes of the systems are small and the two-electron integrals remain constant or change slowly, the k_{ab} can be regarded as a constant. In this case, there is a good linear correlation between the magnetic coupling constant J and the energy difference of

the two singly occupied molecular orbitals ($\Delta = |\varepsilon_a - \varepsilon_s|$) in the triplet state. Therefore, this energy gap $\Delta = |\varepsilon_a - \varepsilon_s|$ can describe the change of the magnetic coupling constant with the system configuration. When $\Delta = |\varepsilon_a - \varepsilon_s|$ is large, the magnetic coupling interaction between the two radical centers is AFM. On the other hand, when $\varepsilon_a = \varepsilon_s$ or $k_{ab} > (|\varepsilon_a - \varepsilon_s|^2)/(J_{aa} - J_{ab})$, the diradical system represents the FM character. Figure 7

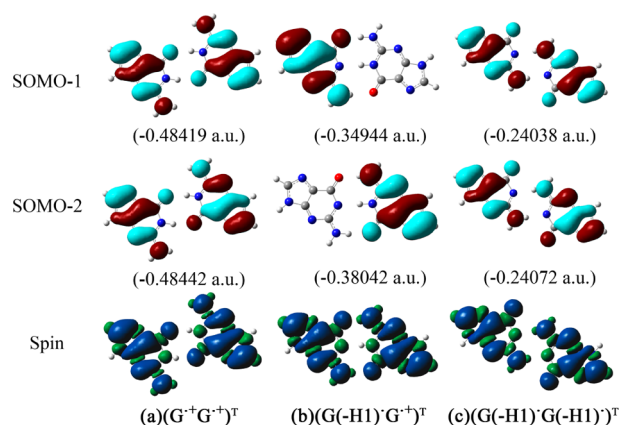


Figure 7. Singly occupied molecular orbitals (first and second rows) and spin density maps (third row) of triplet state of (a) $(\text{G}^{\bullet+}\text{G}^{\bullet+})_{\text{WC}}$, (b) $(\text{G}(\text{-H1})\cdot\text{G}^{\bullet+})_{\text{WC}}$, and (c) $(\text{G}(\text{-H1})\cdot\text{G}(\text{-H1})\cdot)_{\text{WC}}$ base pairs.

illustrates the SOMOs and spin density surfaces of $(\text{G}^{\bullet+}\text{G}^{\bullet+})_{\text{WC}}^{\text{T}}$, $(\text{G}(\text{-H1})\cdot\text{G}^{\bullet+})_{\text{WC}}^{\text{T}}$, and $(\text{G}(\text{-H1})\cdot\text{G}(\text{-H1})\cdot)_{\text{WC}}^{\text{T}}$ and their orbital energies of the two SOMOs. Obviously, for $(\text{G}^{\bullet+}\text{G}^{\bullet+})_{\text{WC}}^{\text{T}}$ and $(\text{G}(\text{-H1})\cdot\text{G}(\text{-H1})\cdot)_{\text{WC}}^{\text{T}}$, the SOMO-1 levels of these two complexes are close to SOMO-2 for the corresponding complexes (−0.48419 versus −0.48442 au for $(\text{G}^{\bullet+}\text{G}^{\bullet+})_{\text{WC}}^{\text{T}}$ and −0.24038 versus −0.24072 au for $(\text{G}(\text{-H1})\cdot\text{G}(\text{-H1})\cdot)_{\text{WC}}^{\text{T}}$), which result in a weak FM interaction for $(\text{G}^{\bullet+}\text{G}^{\bullet+})_{\text{WC}}$ and $(\text{G}(\text{-H1})\cdot\text{G}(\text{-H1})\cdot)_{\text{WC}}$. While for $(\text{G}(\text{-H1})\cdot\text{G}^{\bullet+})_{\text{WC}}^{\text{T}}$, the energy gap of the two SOMOs is relatively large (−0.34944 versus −0.38042 au), which leads to the weak AFM coupling interaction in $(\text{G}(\text{-H1})\cdot\text{G}^{\bullet+})_{\text{WC}}$. This is consistent with the results discussed above. For $(\text{G}^{\bullet+}\text{G}^{\bullet+})_{\text{WC}}$ and $(\text{G}(\text{-H1})\cdot\text{G}(\text{-H1})\cdot)_{\text{WC}}$, their corresponding magnetic orbitals are much similar, their SOMO-1 or SOMO-2 orbitals localize on the two different moieties. However, for $(\text{G}(\text{-H1})\cdot\text{G}^{\bullet+})_{\text{WC}}$, the SOMO-1 resides in one moiety and the SOMO-2 localizes on the other moiety. For these three complexes, the spin densities over the two radical moieties are the α -spin densities. It is obvious that the two radical moieties are indeed the magnetic centers.

The continuum solvation effects were further considered to examine the solvent impact on their ground state properties and diradical characters by using the conductor polarizable continuum model (CPCM) with the dielectric constant of water ($\varepsilon = 78.4$). The single point energy calculations were done on the basis of the CPCM model using the gas phase optimized geometries. As shown in Table S1 and Table S7, for the $\text{G}^{\bullet+}\text{G}^{\bullet+}$ series, the results show that $(\text{G}^{\bullet+}\text{G}^{\bullet+})_{\text{WC}}$ has the triplet ground state, $(\text{G}^{\bullet+}\text{G}^{\bullet+})_{\text{HoogI}}$ has open-shell singlet ground state, and $(\text{G}^{\bullet+}\text{G}^{\bullet+})_{\text{HoogII}}$, $(\text{G}^{\bullet+}\text{G}^{\bullet+})_{\text{minI}}$, $(\text{G}^{\bullet+}\text{G}^{\bullet+})_{\text{minII}}$, $(\text{G}^{\bullet+}\text{G}^{\bullet+})_{\text{minIII}}$, $(\text{G}^{\bullet+}\text{G}^{\bullet+})_{\text{HoHo}}$ are the closed-shell systems, in accordance with those in the gas phase. In the aqueous phase, the binding energies of the $(\text{G}^{\bullet+}\text{G}^{\bullet+})_{\text{WC}}$, $(\text{G}^{\bullet+}\text{G}^{\bullet+})_{\text{HoogI}}$, $(\text{G}^{\bullet+}\text{G}^{\bullet+})_{\text{HoogII}}$, $(\text{G}^{\bullet+}\text{G}^{\bullet+})_{\text{minI}}$, $(\text{G}^{\bullet+}\text{G}^{\bullet+})_{\text{minII}}$, $(\text{G}^{\bullet+}\text{G}^{\bullet+})_{\text{minIII}}$, $(\text{G}^{\bullet+}\text{G}^{\bullet+})_{\text{HoHo}}$ complexes in their ground states are 3.24, 0.24,

15.82, 21.03, 24.39, 26.91, and -1.38 kcal/mol, respectively. Comparing with the binding energies in the gas phase (21.56, 25.31, 39.52, 69.10, 69.94, 70.50, and 31.84 kcal/mol), the binding energies in solution are considerably lower than those in the gas phase. These calculations indicate that the binding ability between $G^{\bullet+}$ and $G^{\bullet+}$ in solution is greatly increased relative to that in the gas phase. What's more, in aqueous solution, for $(G^{\bullet+}G^{\bullet+})_{\text{Hoogl}}$ the spin contamination ($\langle S^2 \rangle = 1.02$) for its open-shell BS singlet state is also close to 1.0, which clearly indicates that the singlet state is the mixture of pure singlet ($\langle S^2 \rangle = 0.0$) and pure triplet state ($\langle S^2 \rangle = 2.0$) (Table S7 of the Supporting Information). This observation indicates that $(G^{\bullet+}G^{\bullet+})_{\text{Hoogl}}$ in aqueous solution also possesses significant diradical character, which is also consistent with the results in the gas phase. For the $(G(-H1) \cdot G^{\bullet+})$ and $(G(-H1) \cdot G(-H1) \cdot)$ series, the relevant energies and spin contamination $\langle S^2 \rangle$ values in aqueous solution are also investigated. Similarly, for the $(G(-H1) \cdot G^{\bullet+})$ series, $(G(-H1) \cdot G(-H1) \cdot)$, $(G(-H1) \cdot G^{\bullet+})_{\text{WC}}$, $(G(-H1) \cdot G^{\bullet+})_{\text{Hoogl}}$, $(G(-H1) \cdot G^{\bullet+})_{\text{minI}}$, $(G(-H1) \cdot G^{\bullet+})_{\text{minII}}$ and $(G(-H1) \cdot G(-H1) \cdot)_{\text{minII}}$ have open-shell BS singlet diradical ground states; $(G(-H1) \cdot G(-H1) \cdot)_{\text{WC}}$, $(G(-H1) \cdot G(-H1) \cdot)_{\text{minI}}$ and $(G(-H1) \cdot G(-H1) \cdot)_{\text{minIII}}$ possess a triplet as their ground states; and $(G(-H1) \cdot G^{\bullet+})_{\text{minIII}}$, $(G(-H1) \cdot G^{\bullet+})_{\text{HoHo}}$ and $(G(-H1) \cdot G(-H1) \cdot)_{\text{HoHo}}$ have the closed-shell singlet ground states, in agreement with the above-discussed gas phase results (Table S1 and Table S7). As a summary, these observations on three series indicate that the ground states in the continuum dielectric media are consistent with those in the gas phase. In addition, these results indicate that the surrounding polarity can change the binding energies but does not change their ground states and diradical characters.

3.2. π - π Stacked $(G^{\bullet+}G^{\bullet+})_{\pi\pi}$, $(G(-H1) \cdot G^{\bullet+})_{\pi\pi}$, and $(G(-H1) \cdot G(-H1) \cdot)_{\pi\pi}$ Complexes. The structural and magnetic characteristics of the π - π stacked $(G^{\bullet+}G^{\bullet+})_{\pi\pi}$, $(G(-H1) \cdot G^{\bullet+})_{\pi\pi}$ and $(G(-H1) \cdot G(-H1) \cdot)_{\pi\pi}$ conformers were also examined. We mainly considered parallel, cross, and antiparallel stacked conformations. According to the relative positions and types of the two bases, the optimized π - π stacked structures can be marked as $(G1G2)^p_{\pi\pi}$, $(G1G2)^{cr}_{\pi\pi}$, $(G1G2)^{ap}_{\pi\pi}$, and $(G1G2)^{cl}_{\pi\pi}$ ($G1, G2 = G^{\bullet+}, G(-H1) \cdot$), in which the superscript p, cr, ap, and cl denote parallel, cross right, antiparallel, and cross left, respectively (Figure 8). We hope the π - π stacked base pairs would also possess novel electronic properties. In the following, we have made a detailed analysis to obtain a basic understanding of the structural and electronic properties that take place in the π - π stacked $(G^{\bullet+}G^{\bullet+})_{\pi\pi}$, $(G(-H1) \cdot G^{\bullet+})_{\pi\pi}$, and $(G(-H1) \cdot G(-H1) \cdot)_{\pi\pi}$ conformers.

A. $(G^{\bullet+}G^{\bullet+})_{\pi\pi}$ Series. For the $(G^{\bullet+}G^{\bullet+})_{\pi\pi}$ series, according to the relative positions, we considered four complexes, labeled as $(G^{\bullet+}G^{\bullet+})^p_{\pi\pi}$, $(G^{\bullet+}G^{\bullet+})^{cr}_{\pi\pi}$, $(G^{\bullet+}G^{\bullet+})^{ap}_{\pi\pi}$ and $(G^{\bullet+}G^{\bullet+})^{cl}_{\pi\pi}$. The optimized geometries of three spin states are given in Figure S33. Overall, for all the spin states of each structure, we can see that only the optimized structures of the open-shell BS singlet for the $(G^{\bullet+}G^{\bullet+})^p_{\pi\pi}$ and $(G^{\bullet+}G^{\bullet+})^{ap}_{\pi\pi}$ complexes still maintain the $\pi\pi$ -stacked conformations similar to their corresponding closed-shell singlet state. For the geometries of the triplet state, $G^{\bullet+}$ binds with $G^{\bullet+}$ through π and carbonyl oxygen interaction or carbonyl oxygen and carbonyl oxygen interaction (σ - π mode or π - π mode), and in fact, those are not their real triplet states. That is to say, when the $(G^{\bullet+}G^{\bullet+})_{\pi\pi}$ conformers are in triplet state, the initial π - π stacked conformations always convert to the σ - π interaction of C=O and the guanine ring or

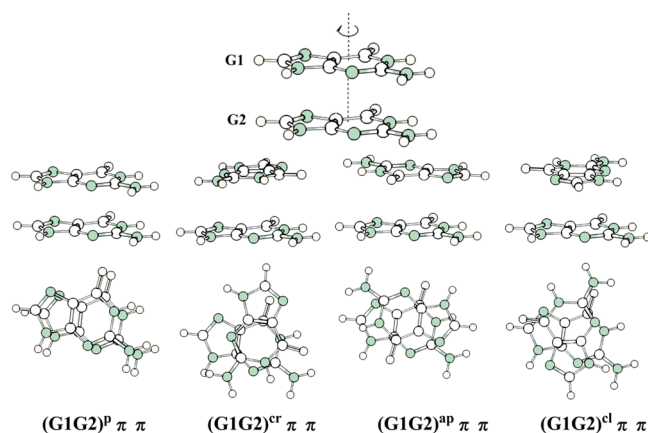


Figure 8. A schematic representation of the $\pi\pi$ -stacked $(G^{\bullet+}G^{\bullet+})_{\pi\pi}$ model. These models can be approximately considered as G1 along the axis rotated about 0° , 90° , 180° , and 270° , respectively, which are labeled as $(G1G2)^p_{\pi\pi}$, $(G1G2)^{cr}_{\pi\pi}$, $(G1G2)^{ap}_{\pi\pi}$ and $(G1G2)^{cl}_{\pi\pi}$. Side- and top views of $\pi\pi$ -stacked $(G1G2)_{\pi\pi}$ complexes in the closed-shell singlet states. G1, G2 represent the guanine radical ($G^{\bullet+}$) and/or dehydrogenated guanine radical ($G(-H1) \cdot$). The $(G^{\bullet+}G^{\bullet+})_{\pi\pi}$ series (including $(G^{\bullet+}G^{\bullet+})^p_{\pi\pi}$, $(G^{\bullet+}G^{\bullet+})^{cr}_{\pi\pi}$, $(G^{\bullet+}G^{\bullet+})^{ap}_{\pi\pi}$ and $(G^{\bullet+}G^{\bullet+})^{cl}_{\pi\pi}$), $(G(-H1) \cdot G^{\bullet+})_{\pi\pi}$ series (including $(G(-H1) \cdot G^{\bullet+})^p_{\pi\pi}$, $(G(-H1) \cdot G^{\bullet+})^{cr}_{\pi\pi}$, $(G(-H1) \cdot G^{\bullet+})^{ap}_{\pi\pi}$ and $(G(-H1) \cdot G^{\bullet+})^{cl}_{\pi\pi}$) and $(G(-H1) \cdot G(-H1) \cdot)_{\pi\pi}$ series (including $(G(-H1) \cdot G(-H1) \cdot)^p_{\pi\pi}$, $(G(-H1) \cdot G(-H1) \cdot)^{cr}_{\pi\pi}$, $(G(-H1) \cdot G(-H1) \cdot)^{ap}_{\pi\pi}$ and $(G(-H1) \cdot G(-H1) \cdot)^{cl}_{\pi\pi}$) are considered.

π - π interaction of C=O and C=O conformations. The short-range coupling interaction of π -radicals overcomes the electrostatic repulsion, which makes these complexes metastable. When in the triplet state, the spin couplings repel each other, and therefore the stacked structures do not exist.

In order to predict their magnetic properties, we calculated the energies of the open-shell BS singlet and triplet states using their corresponding closed-shell singlet structures. For $(G^{\bullet+}G^{\bullet+})^p_{\pi\pi}$, $(G^{\bullet+}G^{\bullet+})^{cr}_{\pi\pi}$, $(G^{\bullet+}G^{\bullet+})^{ap}_{\pi\pi}$ and $(G^{\bullet+}G^{\bullet+})^{cl}_{\pi\pi}$, the energies of the singlet states are lower than those of the triplet states, which indicate that the two electrons prefer to distribute separately with opposite spin directions. The diradical character percentages of $(G^{\bullet+}G^{\bullet+})^p_{\pi\pi}$, $(G^{\bullet+}G^{\bullet+})^{cr}_{\pi\pi}$, $(G^{\bullet+}G^{\bullet+})^{ap}_{\pi\pi}$ and $(G^{\bullet+}G^{\bullet+})^{cl}_{\pi\pi}$ are considered to be 30.1, 53.7, 31.4, and 29.9%, respectively, which indicate that the diradical character appears in the orbital occupation for them (Table S6). The magnetic coupling constants for $(G^{\bullet+}G^{\bullet+})^p_{\pi\pi}$, $(G^{\bullet+}G^{\bullet+})^{cr}_{\pi\pi}$, $(G^{\bullet+}G^{\bullet+})^{ap}_{\pi\pi}$ and $(G^{\bullet+}G^{\bullet+})^{cl}_{\pi\pi}$ are -2523.4 , -1229.6 , -2660.8 , and -2571.9 cm^{-1} , respectively, which clearly indicate the noticeable FM character of these four stacked complexes (Table 4).

B. $(G(-H1) \cdot G^{\bullet+})_{\pi\pi}$ Series. For $(G(-H1) \cdot G^{\bullet+})_{\pi\pi}$, four $\pi\pi$ -stacked conformations together with the distances between $G(-H1) \cdot$ and $G^{\bullet+}$ are given in Figure S34. These conformers are identified as $(G(-H1) \cdot G^{\bullet+})^p_{\pi\pi}$, $(G(-H1) \cdot G^{\bullet+})^{cr}_{\pi\pi}$, $(G(-H1) \cdot G^{\bullet+})^{ap}_{\pi\pi}$ and $(G(-H1) \cdot G^{\bullet+})^{cl}_{\pi\pi}$. Except for $(G(-H1) \cdot G^{\bullet+})^{ap}_{\pi\pi}$, there are significant changes in geometries of the open-shell BS singlet and triplet states relative to their corresponding closed-shell singlet structures.

We also determined their magnetic properties based on their closed-singlet state structures. The relative energies of these spin states for the $(G(-H1) \cdot G^{\bullet+})_{\pi\pi}$ series were calculated and the energy orders for different spin states of them are shown in Table S5. In this group, their ground states are the open-shell singlets. The calculated occupation numbers of LUMO for $(G(-H1) \cdot G^{\bullet+})^p_{\pi\pi}$, $(G(-H1) \cdot G^{\bullet+})^{cr}_{\pi\pi}$, $(G(-H1) \cdot G^{\bullet+})^{ap}_{\pi\pi}$ and $(G(-H1) \cdot G^{\bullet+})^{cl}_{\pi\pi}$ are

Table 4. Energies (kcal/mol) for the Single-Triplet Gaps ($\Delta E_{(T-BS)}$), Differences between Open-Shell Broken-Symmetry Singlet and Closed-Shell RM062X Solution $\Delta E_{(BS-CS)}$, and Intermolecular Magnetic Exchange Coupling Constants J of $(G^{*+}G^{*+})_{\pi\pi}$, $(G(-H1)G^{*+})_{\pi\pi}$, and $(G(-H1)G(-H1))_{\pi\pi}$ Base Pairs Calculated at the M062X/6-311+G* Level^a

$(G^{*+}G^{*+})_{\pi\pi}$	$\Delta E_{(T-BS)}$	$\Delta E_{(BS-CS)}$	J (cm ⁻¹)
$(G^{*+}G^{*+})_{\pi\pi}^p$	10.76	-2.01	-2523.4
$(G^{*+}G^{*+})_{\pi\pi}^{cr}$	4.11	-7.93	-1229.6
$(G^{*+}G^{*+})_{\pi\pi}^{ap}$	11.41	-1.96	-2660.8
$(G^{*+}G^{*+})_{\pi\pi}^{cl}$	11.01	-1.86	-2571.9
$(G(-H1)G^{*+})_{\pi\pi}$	$\Delta E_{(T-BS)}$	$\Delta E_{(BS-CS)}$	J (cm ⁻¹)
$(G(-H1)G^{*+})_{\pi\pi}^p$	3.92	-0.35	-761.7
$(G(-H1)G^{*+})_{\pi\pi}^{cr}$	2.17	-1.78	-498.5
$(G(-H1)G^{*+})_{\pi\pi}^{ap}$	1.35	-0.35	-262.5
$(G(-H1)G^{*+})_{\pi\pi}^{cl}$	2.07	-0.05	-374.4
$(G(-H1)G(-H1))_{\pi\pi}$	$\Delta E_{(T-BS)}$	$\Delta E_{(BS-CS)}$	J (cm ⁻¹)
$(G(-H1)G(-H1))_{\pi\pi}^p$	0.58	-4.84	-186.5
$(G(-H1)G(-H1))_{\pi\pi}^{cr}$	1.49	-8.74	-486.4
$(G(-H1)G(-H1))_{\pi\pi}^{ap}$	4.16	-3.35	-1168.3
$(G(-H1)G(-H1))_{\pi\pi}^{cl}$	-0.44	-3.05	128.7

^aNote: To predict their magnetic properties of the $(G^{*+}G^{*+})_{\pi\pi}$ and $(G(-H1)G^{*+})_{\pi\pi}$ we calculated the energies of the open-shell BS singlet and triplet states based on their corresponding closed-shell singlet structures.

$(H1)G^{*+})_{\pi\pi}^{cl}$ are 0.104, 0.417, 0.102, and 0.225, and consequently the amounts of the diradical character are 10.4%, 41.7%, 10.2%, and 22.5%, respectively, which depict the diradical character quantitatively (Table S6). The energy differences between the singlet and triplet are 3.92, 2.17, 1.35, and 2.07 kcal/mol, and their magnetic coupling constants, the J values of $(G(-H1)G^{*+})_{\pi\pi}^p$, $(G(-H1)G^{*+})_{\pi\pi}^{cr}$, $(G(-H1)G^{*+})_{\pi\pi}^{ap}$, and $(G(-H1)G^{*+})_{\pi\pi}^{cl}$ are -761.7, -498.5, -337.3, and -374.4 cm⁻¹, respectively. These results indicate the AFM character of these complexes and also clearly indicate strong magnetic interactions between two spin centers (Table 4).

C. $(G(-H1)G(-H1))_{\pi\pi}$ Series. We also examined four complexes in the $(G(-H1)G(-H1))_{\pi\pi}$ series, called $(G(-H1)G(-H1))_{\pi\pi}^p$, $(G(-H1)G(-H1))_{\pi\pi}^{cr}$, $(G(-H1)G(-H1))_{\pi\pi}^{ap}$, and $(G(-H1)G(-H1))_{\pi\pi}^{cl}$.

$(H1)G^{*+})_{\pi\pi}^{ap}$ and $(G(-H1)G(-H1))_{\pi\pi}^{cl}$. By optimizing their closed-shell singlet (CS), open-shell BS singlet (BS), and triplet states (T), we find that the geometries of these various spin states still remain parallel, cross left, antiparallel, cross right conformations which are similar to their corresponding initial geometries (as shown in Figure 9). In these conformers, taking the geometries of the singlet and the corresponding triplet states of each structure for comparison, we can see that the main differences occur in distances between two radical moieties, and therefore, the π - π interaction basically changes a little along with the change of distances between two radicals. Their structures show that the distances of G^r and G^r are the order of $r_{CS} < r_{BS} < r_T$ (2.979, 3.321, 3.596 Å for $(G(-H1)G(-H1))_{\pi\pi}^p$; 2.840, 3.058, 3.111 Å for $(G(-H1)G(-H1))_{\pi\pi}^{cr}$; 3.201, 3.203, 3.386 Å for $(G(-H1)G(-H1))_{\pi\pi}^{ap}$; and 2.941, 3.049, 3.191 Å for $(G(-H1)G(-H1))_{\pi\pi}^{cl}$).

For $(G(-H1)G(-H1))_{\pi\pi}^p$, $(G(-H1)G(-H1))_{\pi\pi}^{cr}$, and $(G(-H1)G(-H1))_{\pi\pi}^{ap}$, the results support an open-shell BS singlet ground state for them, according to the energy order of various spin states. In detail, it is clear from Table 4 that their singlet-triplet gaps are 0.58, and 1.49, 4.16 kcal/mol (triplet over singlet), respectively. Meanwhile, the closed-shell singlet state is higher in energy relative to the open-shell BS singlet state. This means that the open-shell BS singlet states are the stable ground states for them. Additionally, the spin contaminations ($\langle S^2 \rangle$) for their singlet states are close to 1.0 (0.95 for $(G(-H1)G(-H1))_{\pi\pi}^p$, 0.97 for $(G(-H1)G(-H1))_{\pi\pi}^{cr}$, 0.79 for $(G(-H1)G(-H1))_{\pi\pi}^{ap}$), and their LUMO occupation numbers are 0.312, 0.457, and 0.307, and thus the diradical percentages are 31.2%, 45.7%, and 30.7%, respectively (Table S6). In all, these observations imply that each of these three molecules possesses an open-shell BS singlet ground state with a large amount of diradical character. However, for $(G(-H1)G(-H1))_{\pi\pi}^{cl}$ we can see from Table 4 that the triplet state is lower than the open-shell BS state by about 0.44 kcal/mol, and the open-shell BS state is more stable than the corresponding closed-shell singlet state with an energy difference of 3.05 kcal/mol. Clearly, $(G(-H1)G(-H1))_{\pi\pi}^{cl}$ has a triplet ground state. It is noteworthy that despite this, its open-shell BS singlet shows interesting diradical character, proven by the calculated spin contamination ($\langle S^2 \rangle = 0.83$), the occupation number of the LUMO (0.297), and the percentage of the diradical character (29.7%). Our calculations reveal that the complexes

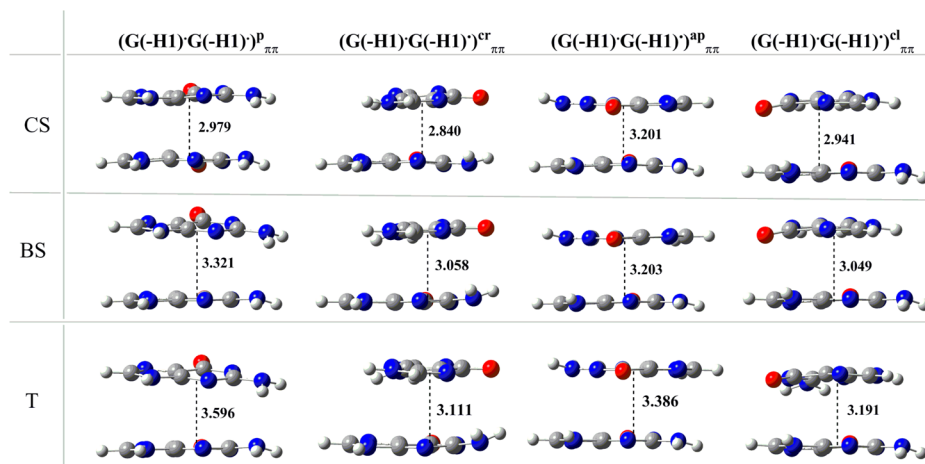


Figure 9. The optimized geometries with indicated bond lengths (Å) for $(G(-H1)G(-H1))_{\pi\pi}^p$, $(G(-H1)G(-H1))_{\pi\pi}^{cr}$, $(G(-H1)G(-H1))_{\pi\pi}^{ap}$, and $(G(-H1)G(-H1))_{\pi\pi}^{cl}$ base pairs. CS, BS, and T denote the closed-shell singlet, open-shell broken-symmetry singlet, and triplet state, respectively.

of this $(G(-H1)^\bullet G(-H1)^\bullet)_{\pi\pi}$ series possess diradical character when they are in the open-shell singlet state. In addition, Figure 10 gives insights into the electronic properties of $(G(-H1)^\bullet G(-H1)^\bullet)_{\pi\pi}$ series in their open-shell BS singlet states.

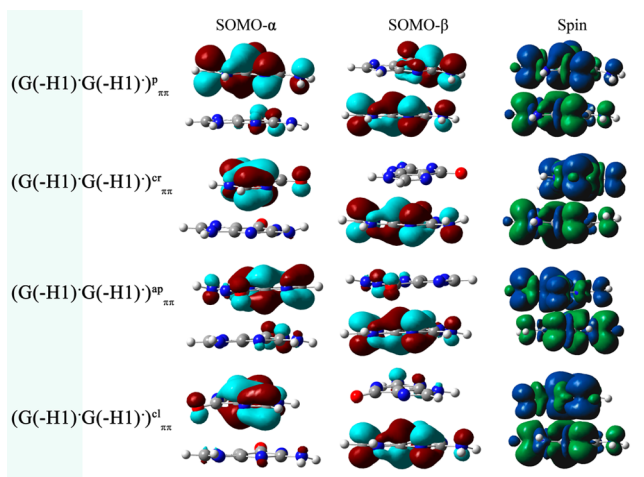


Figure 10. Spin density maps and SOMOs of the $(G(-H1)^\bullet G(-H1)^\bullet)_{\pi\pi}$ series in their open-shell BS singlet states.

$H1)^\bullet)_{\pi\pi}$ by showing the SOMOs and the spin density surfaces. The spin density and orbital analysis shows that the two unpaired electrons are basically localized on the two guanine radical rings separately with opposite spin directions. The situations of other π – π stacked complexes are basically the same.

The J values of $(G(-H1)^\bullet G(-H1)^\bullet)_{\pi\pi}^p$, $(G(-H1)^\bullet G(-H1)^\bullet)_{\pi\pi}^{cr}$, $(G(-H1)^\bullet G(-H1)^\bullet)_{\pi\pi}^{ap}$, and $(G(-H1)^\bullet G(-H1)^\bullet)_{\pi\pi}^{cl}$ are calculated to be -186.5 , -486.4 , -1168.3 , and 128.7 cm^{-1} , respectively. Accordingly, the negative J values indicate that $(G(-H1)^\bullet G(-H1)^\bullet)_{\pi\pi}^p$, $(G(-H1)^\bullet G(-H1)^\bullet)_{\pi\pi}^{cr}$, and $(G(-H1)^\bullet G(-H1)^\bullet)_{\pi\pi}^{ap}$ possess strong AFM coupling, and the positive J for the $(G(-H1)^\bullet G(-H1)^\bullet)_{\pi\pi}^{cl}$ indicates the FM interaction, which correspond with their corresponding ground states.

In summary, for the $(G^{\bullet+}G^{\bullet+})_{\pi\pi}$, $(G(-H1)^\bullet G^{\bullet+})_{\pi\pi}$, and $(G(-H1)^\bullet G(-H1)^\bullet)_{\pi\pi}$ considered here, the quantum chemical calculations indicate that they show obvious magnetic interactions and diradical characters.

4. CONCLUSIONS

We have theoretically studied three series of the double-electron oxidized GG derivatives ($G^{\bullet+}G^{\bullet+}$, $G(-H1)^\bullet G^{\bullet+}$, and $G(-H1)^\bullet G(-H1)^\bullet$), focusing on their relevant geometric and electronic properties, and their spin states and magnetic properties are discussed carefully in this work. It is proved by the unrestricted DFT and CASSCF calculations that $(G^{\bullet+}G^{\bullet+})_{WC}$, $(G(-H1)^\bullet G^{\bullet+})_{minII'}$, $(G(-H1)^\bullet G^{\bullet+})_{minIII'}$, $(G(-H1)^\bullet G(-H1)^\bullet)_{WC}$, $(G(-H1)^\bullet G(-H1)^\bullet)_{minI}$, and $(G(-H1)^\bullet G(-H1)^\bullet)_{minIII}$ have the triplet ground states, whereas $(G^{\bullet+}G^{\bullet+})_{HooGI'}$, $(G(-H1)^\bullet G^{\bullet+})_{WC}$, $(G(-H1)^\bullet G^{\bullet+})_{HooGI'}$, $(G(-H1)^\bullet G^{\bullet+})_{minI}$, and $(G(-H1)^\bullet G(-H1)^\bullet)_{minII}$ possess the open-shell broken-symmetry singlet ground states with diradical characters, and $(G^{\bullet+}G^{\bullet+})_{HooGI'}$, $(G^{\bullet+}G^{\bullet+})_{minI}$, $(G^{\bullet+}G^{\bullet+})_{minII}$, $(G^{\bullet+}G^{\bullet+})_{minIII}$, $(G^{\bullet+}G^{\bullet+})_{HoHo'}$, $(G(-H1)^\bullet G^{\bullet+})_{HoHo'}$, and $(G(-H1)^\bullet G(-H1)^\bullet)_{HoHo'}$ are the closed-shell systems. However, the magnetic interactions of the H-bonded diradical base pairs are relatively weak, especially in the diradical $G^{\bullet+}G^{\bullet+}$ series and $G(-H1)^\bullet G(-H1)^\bullet$ series. The magnetic coupling interactions of the

diradical systems are controlled by intermolecular interactions (H-bond, electrostatic repulsion, and radical coupling). Orbital analyses show that the HOMO–LUMO gaps of the complexes which have the open-shell ground states are so small that they could allow the promotion of an electron to generate a diradical more easily. The diradical characteristics and magnetic properties in the π – π stacked di-ionized GG base pairs ($(G^{\bullet+}G^{\bullet+})_{\pi\pi}$, $(G(-H1)^\bullet G^{\bullet+})_{\pi\pi}$, and $(G(-H1)^\bullet G(-H1)^\bullet)_{\pi\pi}$) are also considered, and most of them manifest AFM character.

This work provides the first theoretical prediction that some di-ionized GG base pairs possess diradical characters with variable degrees of FM and AFM characters, depending on the dehydrogenation characters of the base and their interaction modes. As discussed above, the results reveal that these radicalized base pairs ($G^{\bullet+}G^{\bullet+}$, $G(-H1)^\bullet G^{\bullet+}$, and $G(-H1)^\bullet G(-H1)^\bullet$), which consist of two radicals ($G^{\bullet+}$ or $G(-H1)^\bullet$) on a variety of the binding modes exhibit different degrees of magnetic characters (FM, AFM, or nonmagnetic properties). Clearly, the two-electron oxidation may lead to the appearance of magnetic properties, compared with their corresponding natural and one-electron oxidized base pairs. Although it is not all interacting modes of the coupled two radicals that lead to diradical and magnetic characters, we still hope that these variable magnetic characteristics can be utilized as an important basis for the identification of the two-electron oxidized GG base pairs. In other words, the magnetic properties reported in this work might be in connection with the question how to judge the di-ionized GG base pair derivatives, and further examination of the predictions needs to be explored. This work would provide useful information for an atomistic understanding of the electronic structures and properties of possible intermediates or products of the di-ionized GG base pairs.

■ ASSOCIATED CONTENT

Supporting Information

Computational data and figures including geometrical parameters, singlet–triplet gaps, occupation number of LUMO, magnetic coupling constants, SOMOs and spin density maps, and others. This material is available free of charge via the Internet at <http://pubs.acs.org>.

■ AUTHOR INFORMATION

Corresponding Author

*E-mail: byx@sdu.edu.cn.

Notes

The authors declare no competing financial interest.

■ ACKNOWLEDGMENTS

This work was supported by NSFC (20633060, 20973101), NCET, and the Independent Innovation Foundation (2009JC020) of Shandong University. Part of the calculations were carried out at the Shanghai Supercomputer Center, the National Supercomputer Center in Jinan, and the High-Performance Computational Platform at SDU-Chem.

■ REFERENCES

- (1) Becker, D.; Sevilla, M. D. The Chemical Consequences of Radiation Damage to DNA. *Adv. Radiat. Biol.* **1993**, *17*, 121–180.
- (2) Burrows, C. J.; Muller, J. G. Oxidative Nucleobase Modifications Leading to Strand Scission. *Chem. Rev.* **1998**, *98*, 1109–1152.
- (3) Angelov, D.; Spassky, A.; Berger, M.; Cadet, J. High-Intensity UV Laser Photolysis of DNA and Purine 2'-Deoxyribonucleosides:

Formation of 8-Oxopurine Damage and Oligonucleotide Strand Cleavage as Revealed by HPLC and Gel Electrophoresis Studies. *J. Am. Chem. Soc.* **1997**, *119*, 11373–11380.

(4) Melvin, T.; Botchway, S. W.; Parker, A. W.; O'Neill, P. Induction of Strand Breaks in Single-Stranded Polyribonucleotides and DNA by Photoionization: One Electron Oxidized Nucleobase Radicals as Precursors. *J. Am. Chem. Soc.* **1996**, *118*, 10031–10036.

(5) Görner, H. New Trends in Photobiology: Photochemistry of DNA and Related Biomolecules: Quantum Yields and Consequences of Photoionization. *J. Photochem. Photobiol., B* **1994**, *26*, 117–139.

(6) Nikogosyan, D. N. Two-Quantum UV Photochemistry of Nucleic Acids: Comparison with Conventional Low-intensity UV Photochemistry and Radiation Chemistry. *Int. J. Radiat. Biol.* **1990**, *57*, 233–299.

(7) Loft, S.; Poulsen, H. E. Cancer Risk and Oxidative DNA Damage in Man. *J. Mol. Med.* **1996**, *74*, 297–312.

(8) Mecocci, P.; Fanó, G.; Fulle, S.; MacGarvey, U.; Shinobu, L.; Polidori, M. C.; Cherubini, A.; Vecchiet, J.; Senin, U.; Beal, M. F. Age-Dependent Increases in Oxidative Damage to DNA, Lipids, and Proteins in Human Skeletal Muscle. *Free Radical Biol. Med.* **1999**, *26*, 303–308.

(9) Richardson, N. A.; Wesolowski, S. S.; Schaefer, H. F. The Adenine–Thymine Base Pair Radical Anion: Adding an Electron Results in a Major Structural Change. *J. Phys. Chem. B* **2003**, *107*, 848–853.

(10) Richardson, N. A.; Wesolowski, S. S.; Schaefer, H. F. Electron Affinity of The Guanine–Cytosine Base Pair and Structural Perturbations upon Anion Formation. *J. Am. Chem. Soc.* **2002**, *124*, 10163–10170.

(11) Bera, P. P.; Schaefer, H. F. (G-H)[•]-C and G-(C-H)[•] radicals derived from the Guanine–Cytosine Base Pair Cause DNA Subunit Lesions. *Proc. Natl. Acad. Sci. U.S.A.* **2005**, *102*, 6698–6703.

(12) Lind, M. C.; Bera, P. P.; Richardson, N. A.; Wheeler, S. E.; Schaefer, H. F. The Deprotonated Guanine–Cytosine Base Pair. *Proc. Natl. Acad. Sci. U.S.A.* **2006**, *103*, 7554–7559.

(13) Kim, S.; Lind, M. C.; Schaefer, H. F. Structures and Energetics of the Deprotonated Adenine–Uracil Base Pair, Including Proton-Transferred Systems. *J. Phys. Chem. B* **2008**, *112*, 3545–3551.

(14) Luo, Q.; Li, J.; Shu, Li, Q.; Kim, S.; Wheeler, S. E.; Xie, Y.; Schaefer, H. F. Electron Affinities of the Radicals Derived from Cytosine. *Phys. Chem. Chem. Phys.* **2005**, *7*, 861–865.

(15) Profeta, L. T. M.; Larkin, J. D.; Schaefer, H. F. The Thymine Radicals and Their Respective Anions: Molecular Structures and Electron Affinities. *Mol. Phys.* **2003**, *101*, 3277–3284.

(16) Dulčić, A.; Herak, J. N. Crystal Structure Dependence of Radiation-Induced Radicals in Thymine: An ESR Study. *Radiat. Res.* **1971**, *47*, 573–580.

(17) Bergene, R.; Melø, T. B. Formation and Trapping of Radical Pairs in Irradiated Thymine. *Int. J. Radiat. Biol.* **1973**, *23*, 263–270.

(18) Dulčić, A.; Herak, J. N. Radiation-Induced Pair-Wise Radical Formation in Single Crystals of Thymine. *Biochim. Biophys. Acta* **1973**, *319*, 109–115.

(19) Peoples, A. R.; Mercer, K. R.; Bernhard, W. A. What Fraction of DNA Double-Strand Breaks Produced by the Direct Effect is Accounted for by Radical Pairs? *J. Phys. Chem. B* **2010**, *114*, 9283–9288.

(20) Becker, D.; Adhikary, A.; Tetteh, S. T.; Bull, A. W.; Sevilla, M. D. Kr-86 Ion-Beam Irradiation of Hydrated DNA: Free Radical and Unaltered Base Yields. *Radiat. Res.* **2012**, *178*, 524–537.

(21) Weiland, B.; Hüttermann, J. J. Free Radicals from Lyophilized 'Dry' DNA Bombarded with Heavy-Ions as Studied by Electron Spin Resonance Spectroscopy. *Int. J. Radiat. Biol.* **1999**, *75*, 1169–1175.

(22) Prise, K.; Gillies, N.; Michael, B. Further Evidence for Double-Strand Breaks Originating from a Paired Radical Precursor from Studies of Oxygen Fixation Processes. *Radiat. Res.* **1999**, *151*, 635–641.

(23) Pottiboyina, V.; Kumar, A.; Sevilla, M. D. Formation of N–N Cross-Links in DNA by Reaction of Radiation-Produced DNA Base

Pair Diradicals: A DFT Study. *J. Phys. Chem. B* **2011**, *115*, 15090–15097.

(24) Seal, P.; Jha, P. C.; Ågren, H.; Chakrabarti, S. Magnetic Interactions in Dehydrogenated Guanine–Cytosine Base Pair. *Chem. Phys. Lett.* **2008**, *465*, 285–289.

(25) Douki, T.; Cadet, J. Modification of DNA Bases by Photosensitized One-Electron Oxidation. *Int. J. Radiat. Biol.* **1999**, *75*, 571–581.

(26) Kupan, A.; Saulière, A.; Broussy, S.; Seguy, C.; Pratviel, G.; Meunier, B. Guanine Oxidation by Electron Transfer: One- versus Two-Electron Oxidation Mechanism. *ChemBioChem* **2006**, *7*, 125–133.

(27) Misiaszek, R.; Crean, C.; Joffe, A.; Geacintov, N. E.; Shafirovich, V. Oxidative DNA Damage Associated with Combination of Guanine and Superoxide Radicals and Repair Mechanisms via Radical Trapping. *J. Biol. Chem.* **2004**, *279*, 32106–32115.

(28) Kobayashi, K.; Tagawa, S. Direct Observation of Guanine Radical Cation Deprotonation in Duplex DNA Using Pulse Radiolysis. *J. Am. Chem. Soc.* **2003**, *125*, 10213–10218.

(29) Adhikary, A.; Kumar, A.; Becker, D.; Sevilla, M. D. The Guanine Cation Radical: Investigation Of Deprotonation States by ESR and DFT. *J. Phys. Chem. B* **2006**, *110*, 24171–24180.

(30) Adhikary, A.; Khanduri, D.; Sevilla, M. D. Direct Observation of the Hole Protonation State And Hole Localization Site in DNA-Oligomers. *J. Am. Chem. Soc.* **2009**, *131*, 8614–8619.

(31) Adhikary, A.; Kumar, A.; Munafo, S. A.; Khanduri, D.; Sevilla, M. D. Prototropic Equilibria in DNA Containing One-Electron Oxidized GC: Intra-Duplex vs. Duplex to Solvent Deprotonation. *Phys. Chem. Chem. Phys.* **2010**, *12*, 5353–5368.

(32) Khanduri, D.; Adhikary, A.; Sevilla, M. D. Highly Oxidizing Excited States of One-Electron-Oxidized Guanine in DNA: Wavelength and pH Dependence. *J. Am. Chem. Soc.* **2011**, *133*, 4527–4537.

(33) Candéias, L. P.; Steenken, S. Structure and Acid-Base Properties of One-Electron-Oxidized Deoxyguanosine, Guanosine, and 1-Methylguanosine. *J. Am. Chem. Soc.* **1989**, *111*, 1094–1099.

(34) Kobayashi, K.; Yamagami, R.; Tagawa, S. Effect of Base Sequence and Deprotonation of Guanine Cation Radical in DNA. *J. Phys. Chem. B* **2008**, *112*, 10752–10757.

(35) Naumov, S.; von Sonntag, C. Guanine-Derived Radicals: Dielectric Constant-Dependent Stability and UV/Vis Spectral Properties: A DFT Study. *Radiat. Res.* **2008**, *169*, 364–372.

(36) Mundy, C. J.; Colvin, M. E.; Quong, A. A. Irradiated Guanine: A Car-Parrinello Molecular Dynamics Study of Dehydrogenation in the Presence of an OH Radical. *J. Phys. Chem. A* **2002**, *106*, 10063–10071.

(37) Jena, N. R.; Mishra, P. C. Interaction of Guanine, Its Anions, and Radicals with Lysine in Different Charge States. *J. Phys. Chem. B* **2007**, *111*, 5418–5424.

(38) Kubičková, A.; Křížek, T. s.; Coufal, P.; Wernersson, E.; Heyda, J.; Jungwirth, P. Guanidinium Cations Pair with Positively Charged Arginine Side Chains in Water. *J. Phys. Chem. Lett.* **2011**, *2*, 1387–1389.

(39) Vazdar, M.; Uhlig, F.; Jungwirth, P. Like-Charge Ion Pairing in Water: An Ab Initio Molecular Dynamics Study of Aqueous Guanidinium Cations. *J. Phys. Chem. Lett.* **2012**, *3*, 2021–2024.

(40) Vondrášek, J. i.; Mason, P. E.; Heyda, J.; Collins, K. D.; Jungwirth, P. The Molecular Origin of Like-Charge Arginine–Arginine Pairing in Water. *J. Phys. Chem. B* **2009**, *113*, 9041–9045.

(41) No, K. T.; Nam, K.-Y.; Scheraga, H. A. Stability of Like and Oppositely Charged Organic Ion Pairs in Aqueous Solution. *J. Am. Chem. Soc.* **1997**, *119*, 12917–12922.

(42) Mason, P. E.; Neilson, G. W.; Enderby, J. E.; Sabounji, M.-L.; Dempsey, C. E.; MacKerell, A. D.; Brady, J. W. The Structure of Aqueous Guanidinium Chloride Solutions. *J. Am. Chem. Soc.* **2004**, *126*, 11462–11470.

(43) Becker, D.; Razskazovskii, Y.; Callaghan, M. U.; Sevilla, M. D. Electron Spin Resonance of DNA Irradiated with a Heavy-Ion Beam (¹⁶O⁸⁺): Evidence for Damage to the Deoxyribose Phosphate Backbone. *Radiat. Res.* **1996**, *146*, 361–368.

- (44) Becker, D.; Bryant-Friedrich, A.; Trzasko, C.; Sevilla, M. D. Electron Spin Resonance Study of DNA Irradiated with an Argon-Ion Beam: Evidence for Formation of Sugar Phosphate Backbone Radicals. *Radiat. Res.* **2003**, *160*, 174–185.
- (45) Becke, A. D. A New Mixing of Hartree-Fock and Local Density-Functional Theories. *J. Chem. Phys.* **1993**, *98*, 1372–1377.
- (46) Boys, S. F.; Bernardi, F. The Calculation of Small Molecular Interactions by the Differences of Separate Total Energies. Some Procedures with Reduced Errors. *Mol. Phys.* **1970**, *19*, 553–566.
- (47) Zhao, Y.; Schultz, N. E.; Truhlar, D. G. Design of Density Functionals by Combining the Method of Constraint Satisfaction with Parametrization for Thermochemistry, Thermochemical Kinetics, and Noncovalent Interactions. *J. Chem. Theory Comput.* **2006**, *2*, 364–382.
- (48) Zhao, Y.; Truhlar, D. The M06 Suite of Density Functionals for Main Group Thermochemistry, Thermochemical Kinetics, Non-covalent Interactions, Excited States, and Transition Elements: Two New Functionals and Systematic Testing of Four M06-Class Functionals and 12 Other Functionals. *Theor. Chem. Acc.* **2008**, *120*, 215–241.
- (49) Noodleman, L. Valence Bond Description of Antiferromagnetic Coupling in Transition Metal Dimers. *J. Chem. Phys.* **1981**, *74*, 5737–5743.
- (50) Noodleman, L.; Baerends, E. J. Electronic Structure, Magnetic Properties, ESR, and Optical Spectra For 2-Iron Ferredoxin Models by LCAO- $X\alpha$ Valence Bond Theory. *J. Am. Chem. Soc.* **1984**, *106*, 2316–2327.
- (51) Yamaguchi, K.; Takahara, Y.; Fueno, T.; Nasu, K. Ab Initio MO Calculations of Effective Exchange Integrals between Transition-Metal Ions via Oxygen Dianions: Nature of the Copper-Oxygen Bonds and Superconductivity. *Jpn. J. Appl. Phys.* **1987**, *26*, L1362.
- (52) Yamaguchi, K.; Jensen, F.; Dorigo, A.; Houk, K. N. A Spin Correction Procedure for Unrestricted Hartree-Fock and Møller-Plesset Wavefunctions for Singlet Diradicals and Polyradicals. *Chem. Phys. Lett.* **1988**, *149*, 537–542.
- (53) Roos, B. O. The Complete Active Space SCF Method in a Fock-Matrix-Based Super-CI Formulation. *Int. J. Quantum Chem.* **1980**, *18*, 175–189.
- (54) Frisch, M. J.; Trucks, G. W.; Schlegel, H. B.; Scuseria, G. E.; Robb, M. A.; Cheeseman, J. R.; Scalmani, G.; Barone, B.; Mennucci, B.; Petersson, H., et al. *Gaussian 09*; Gaussian, Inc.: Wallingford, CT, 2010.
- (55) Shimizu, A.; Kubo, T.; Uruichi, M.; Yakushi, K.; Nakano, M.; Shiomi, D.; Sato, K.; Takui, T.; Hirao, Y.; Matsumoto, K.; et al. Alternating Covalent Bonding Interactions in a One-Dimensional Chain of a Phenalenyl-Based Singlet Biradical Molecule Having Kekulé Structures. *J. Am. Chem. Soc.* **2010**, *132*, 14421–14428.
- (56) Kubo, T.; Katada, Y.; Shimizu, A.; Hirao, Y.; Sato, K.; Takui, T.; Uruichi, M.; Yakushi, K.; Haddon, R. C. Synthesis, Crystal Structure, and Physical Properties of Sterically Unprotected Hydrocarbon Radicals. *J. Am. Chem. Soc.* **2011**, *133*, 14240–14243.
- (57) Bendikov, M.; Duong, H. M.; Starkey, K.; Houk, K. N.; Carter, E. A.; Wudl, F. Oligoacenes: Theoretical Prediction of Open-Shell Singlet Diradical Ground States. *J. Am. Chem. Soc.* **2004**, *126*, 7416–7417.